

1 **Reply to the Interactive comment of Anonymous Referee on “Processes controlling the**
2 **seasonal variations of ^{210}Pb and ^7Be at the Mt. Cimone WMO-GAW global station, Italy:**
3 **A model analysis” by Erika Brattich et al.**

4
5 Manuscript Ref: acp-2016-568

6
7 We thank the reviewer for the further comments. Below please find our responses.

8
9 1) Both reviewers pointed the importance of the station-based observations of precipitation at
10 Mt Cimone for the analysis of the local Be-7 and Pb-210 measurements and the need to show
11 these data even as supplementary material if not in Figure 4. The reviewers pointed this in order
12 to help the reader to see how the difference between the station-based observations of
13 precipitation at Mt Cimone and large scale grid-based precipitation data (MERRA and GPCP)
14 could partially explain differences between the locally observed Be-7 and Pb-210
15 measurements and the respective modeled values. Could the authors please clarify why they
16 prefer not showing these data?

17
18 Reply - As we have previously discussed in the manuscript (page 15, lines 18-21), it is true that
19 the difference between the station-based observations of precipitation and large scale grid-
20 based precipitation data (MERRA and GPCP) could contribute to the biases in our model
21 simulated Be-7 and Pb-210 due to errors in the precipitation scavenging of radionuclides. We
22 thus report in the text annual mean differences between the local observations and MERRA
23 precipitation. We believe this is adequate and showing a figure does not provide additional
24 useful information. Our corresponding text reads “Large differences between the MERRA
25 precipitation and that locally observed at the station are instead present. While the daily mean

1 observed 2005 precipitation is 0.81 mm, which is close to the corresponding precipitation (0.73
2 mm) in MERRA at the “ij” grid (i.e., a negative bias of -0.08 mm); the model bias is positive
3 and much higher (0.31 – 1.28 mm) at adjacent grids. This bias may very well reflect again the
4 fact that the observed surface precipitation is localized, whereas the satellite and MERRA
5 precipitations correspond to a much larger scale (about 200 km).”

6
7 2) The authors added in the manuscript that " However, MERRA is able to capture the
8 summertime north-north easterly winds in the eastern Mediterranean (Aegean Sea), known as
9 the Etesian winds, generated by thermal effects.” The part of the sentence " generated by
10 thermal effects" is a rather incomplete statement. The Etesian winds are one of the most
11 persistent localized wind system in the world as a consequence of a sharp east–west pressure
12 gradient manifested by large scale circulation features (low pressures over eastern
13 Mediterranean/Middle East and high pressure over central and southeastern Europe) (Dafka et
14 al., Clim Dyn, 2015).

15
16 Reply - We thank the reviewer for pointing this out to us. We have revised the manuscript as
17 follows: “However, MERRA is able to capture the summertime north-north easterly winds in
18 the eastern Mediterranean (Aegean Sea), known as the Etesians. The Etesians are the most
19 persistent localized wind system in the world as a result of a sharp east–west pressure gradient
20 manifested by large-scale circulation features (i.e., low pressure over the eastern
21 Mediterranean/Middle East and high pressure over central and southeastern Europe) (Dafka et
22 al., 2016)”. The following paper has been added to the list of references: Dafka, S., Xoplaki,
23 E., Toreti, A., Zanis, P., Tyrlis, E., Zerefos, C., and Luterbacher,

1 J., 2016: The Etesians; from observations to reanalysis. *Clim. Dyn.*, 47, 1569-1585,
2 doi:10.1007/s00382-015-2920-7.

3

4

5 Processes controlling the seasonal variations of ^{210}Pb and ^7Be
6 at the Mt. Cimone WMO-GAW global station, Italy: A model
7 analysis

8 Erika Brattich¹, Hongyu Liu², Laura Tositti¹, David B. Considine³, and James H. Crawford⁴

9 [1] Department of Chemistry “G Ciamician”, Alma Mater Studiorum University of
10 Bologna, Bologna (BO), 40126, Italy

11 [2] National Institute of Aerospace, Hampton, Virginia, Virginia, VA 23681, USA

12 [3] NASA Headquarters, Washington, DC 20546, USA

13 [4] NASA Langley Research Center, Hampton, Virginia, VA 23681, USA

14

15 **Correspondence to:** Hongyu Liu (hongyu.liu-1@nasa.gov)

16 **Abstract.** We apply the Global Modeling Initiative (GMI) chemistry and transport model
17 driven by the NASA’s MERRA assimilated meteorological data to simulate the seasonal
18 variations of two radionuclide aerosol tracers (terrestrial ^{210}Pb and cosmogenic ^7Be) at the
19 WMO-GAW station of Mt. Cimone (44°12’ N, 10°42’ E, 2165 m asl, Italy), which is
20 representative of free-tropospheric conditions most of the year, during 2005 with an aim to
21 understand the roles of transport and precipitation scavenging processes in controlling their
22 seasonality. The total precipitation field in the MERRA data set is evaluated with the Global

1 Precipitation Climatology project (GPCP) observations, and a generally good agreement is
2 found. The model reproduces reasonably the observed seasonal pattern of ^{210}Pb concentrations,
3 characterized by a wintertime minimum due to lower ^{222}Rn emissions and weaker uplift from
4 the boundary layer and summertime maxima resulting from strong convection over the
5 continent. The observed seasonal behavior of ^7Be concentrations shows a winter minimum, a
6 summer maximum, and a secondary spring maximum. The model captures the observed ^7Be
7 pattern in winter-spring, which is linked to the larger stratospheric influence during spring.
8 However, the model tends to underestimate the observed ^7Be concentrations in summer,
9 partially due to the sensitivity to spatial sampling in the model. Model sensitivity experiments
10 indicate a dominant role of precipitation scavenging (versus dry deposition and convection) in
11 controlling the seasonality of ^{210}Pb and ^7Be concentrations at Mt. Cimone.

12

13 **1 Introduction**

14 The use of atmospheric radionuclides to understand atmospheric dynamics, pollution
15 transport and removal processes has a long history (e.g., Junge, 1963; Reiter et al., 1971;
16 Gaggeler, 1995; Arimoto et al., 1999; Turekian and Graustein, 2003; WMO-GAW, 2004; Dibb,
17 2007; Rastogi and Sarin, 2008; Froehlich and Masarik, 2010; Lozano et al., 2012). It has been
18 recognized that natural radionuclides are useful in a global monitoring network for atmospheric
19 composition to support global climate change and air quality research, and therefore they are
20 measured at many of the regional, global and contributing-partner stations in the Global
21 Atmosphere Watch (GAW) network of the World Meteorological Organization (WMO)
22 (WMO-GAW, 2004). In particular, terrigenous ^{210}Pb and cosmogenic ^7Be natural radionuclides
23 are helpful in the understanding of the roles of transport and/or scavenging in controlling the
24 behaviors of radiatively active trace gases and aerosols (Feichter et al., 1991; Balkanski et al.,
25 1993; Koch et al., 1996), as well as their anthropogenic (vs. natural) origin (e.g., Graustein and

1 Turekian, 1996; Arimoto et al., 1999; Liu et al., 2004; Cuevas et al., 2013). They are routinely
2 monitored at WMO-GAW stations around the world (Lee et al., 2004). Although ^{210}Pb and ^7Be
3 have long (1998-2011) been measured at the Global WMO-GAW station of Mt. Cimone (Italy),
4 their seasonal behavior has not been thoroughly elucidated (Lee et al., 2007; Tositti et al.,
5 2014). Here we apply a state-of-the-art global chemistry and transport model (CTM) to the
6 simulation of ^{210}Pb and ^7Be , with an objective to better understand the roles of transport and
7 precipitation scavenging processes in controlling their seasonal variations at Mt. Cimone.

8 Because of their contrasting natural origins, ^{210}Pb and ^7Be have been used as a pair to
9 study the vertical transport and scavenging of aerosols (Koch et al., 1996). ^{210}Pb (half-life $\tau_{1/2}$
10 = 22.3 years) is the decay daughter of ^{222}Rn ($\tau_{1/2} = 3.8$ days), which is emitted from soils by
11 decay of ^{226}Ra . The oceanic input of ^{222}Rn is about two orders of magnitude less than the
12 continental input and, because of the continental origin of ^{222}Rn , ^{210}Pb is considered as a tracer
13 of air masses with continental origin (Baskaran, 2011). ^7Be ($\tau_{1/2} = 53.3$ days) is a cosmogenic
14 radionuclide generated by cosmic ray spallation reactions with nitrogen and oxygen (Lal et al.,
15 1958). Most (~67%) of ^7Be is produced in the stratosphere and the remaining (~33%) is
16 generated in the troposphere, particularly in the upper troposphere (Johnson and Viezee, 1981;
17 Usoskin and Kovaltsov, 2008). ^7Be is thus considered a tracer of stratospheric influence
18 (Vieze and Singh, 1980; Dibb et al., 1992, 1994; Liu et al., 2004, 2016) and subsidence (Feely
19 et al., 1989; Koch et al., 1996; Liu et al., 2004). Once produced, both radionuclides rapidly
20 attach to ubiquitous submicron aerosol particles in the ambient air (Papastefanou and
21 Ioannidou, 1995; Winkler et al., 1998; Gaffney et al., 2004; Ioannidou et al., 2005), and are
22 removed from the atmosphere mainly by wet and secondarily dry deposition (Kulan et al.,
23 2006). The concentrations of these radionuclides in surface air thus depend on their sources,
24 transport, wet and dry removal, and radioactive decay (in the case of ^7Be). Rainfall scavenging

1 processes are generally more effective on ^{210}Pb than on ^7Be concentrations (Koch et al., 1996;
2 Caillet et al., 2001; Likuku, 2006; Dueñas et al., 2009; Lozano et al., 2012).

3 Observational studies have previously been conducted to examine the factors influencing
4 surface ^{210}Pb and ^7Be concentrations in Europe, the Middle East and North Africa. Different
5 synoptic and mesoscale patterns are associated with the ranges of ^{210}Pb and ^7Be activity
6 concentrations (Lozano et al., 2012, 2013). In southwestern Spain (El Arenosillo), for instance,
7 low ^{210}Pb values are strongly linked to air masses from the Atlantic Ocean, whereas the highest
8 values are associated with air masses clearly under the influence of continents, such as the
9 Iberian Peninsula and North of Africa (Lozano et al., 2012). As for ^7Be , the highest ^7Be activity
10 concentrations over southwestern Iberian Peninsula are related with the arrival of air masses
11 from middle latitudes, and in particular from the Canary Islands, western Mediterranean Basin
12 and the north of Africa (Dueñas et al., 2011; Lozano et al., 2012).

13 With respect to ^{210}Pb and ^7Be spatial variability, ^{210}Pb concentrations in surface air are
14 strongly dependent on whether it is located over land or ocean, whereas ^7Be concentration is
15 mainly latitudinally dependent, due to their different production mechanisms. Generally
16 speaking, in the Northern Hemisphere higher ^7Be concentrations are present at middle latitudes
17 (20-50° N), because of the mixing of stratospheric air into the upper troposphere along the
18 tropopause discontinuity in mid-latitude regions and subsequent convective mixing within the
19 troposphere, which brings ^7Be -rich air masses into the planetary boundary layer and to the
20 earth's surface (Kulan et al., 2006). Lower ^7Be concentrations are towards the pole and towards
21 the equator (Kulan et al., 2006; Steinmann et al., 2013).

22 Many studies examined the seasonal behavior of ^{210}Pb and ^7Be at European mid-latitude
23 surface sites (e.g., Cannizzaro et al., 1999; Ioannidou et al., 2005; Daish et al., 2005; Todorovic
24 et al., 2005; Likuku, 2006; Dueñas et al., 2009; Pham et al., 2011; Carvalho et al., 2013;

1 Steinmann et al., 2013). High levels of ^{210}Pb during summer and low levels in winter were
2 found, reflecting the differing rates of ^{222}Rn emanation from soil above the European land mass
3 during winter (wet or snow covered soil) and summer (dry soil) (Hötzl and Winkler, 1987;
4 Caillet et al., 2001; Daish et al., 2005; Ioannidou et al., 2005). At low-elevation sites, monthly
5 ^7Be averages are characterized by a well-defined annual cycle with lower values during winter
6 and higher values during summer. Generally, the increase of ^7Be in ground level air from March
7 to May is ascribed to the more efficient and higher frequency stratosphere- troposphere
8 exchange (STE), whereas the further increase of ^7Be during summer is due to the stronger
9 convective mixing and higher tropopause (Ioannidou et al., 2014). The higher tropopause
10 height is associated with anticyclonic conditions, which results in downward transport from the
11 upper troposphere and reduced wet scavenging during these conditions (Gerasopoulos et al.,
12 2001, 2005; Ioannidou et al., 2014). In fact, compensating subsidence associated with
13 convective mixing enhances downward transport of ^7Be from the upper troposphere (rather
14 than direct input of stratospheric air) down to the lower troposphere and ground level (Zanis et
15 al., 1999; Gerasopoulos et al., 2001, 2005; Ioannidou et al., 2005; Likuku et al., 2006;
16 Steinmann et al., 2013).

17 High-elevation sites such as Jungfrauoch (Switzerland), Zugspitze (Germany), and Mt.
18 Cimone (Italy), typically lying above the planetary boundary layer (PBL), are characterized by
19 lower ^{210}Pb concentrations and higher ^7Be due to direct influences of air masses from the free
20 troposphere (Zanis et al., 2000). The observed seasonal ^{210}Pb pattern at the high-altitude sites
21 of Puy de Dome (1465 m asl, France) and Opme (660 m asl, France) is characterized by
22 maximum concentrations in spring and autumn and minimum concentrations in winter. This is
23 due to higher radon emissions during the dry season (summer) than during the wet season
24 (winter), and lower PBL height during winter (Bourcier et al., 2011). The latter results in
25 weaker upward transport of ^{222}Rn and ^{210}Pb at high-altitude sites. Similar to low-elevation sites,

1 higher ^7Be values are observed in summer due to convection-forced exchange with the upper
2 troposphere and to the higher tropopause height that leads to more efficient vertical transport
3 from the upper to lower troposphere (Reiter et al., 1983; Gerasopoulos et al., 2001; Bourcier et
4 al., 2011). At high-altitude sites a secondary maximum of ^7Be during cold months (December-
5 March) is generally observed and attributed to the increase in stratosphere-to-troposphere
6 events during this season (e.g., James et al., 2003; Stohl et al., 2003; Trickl et al., 2010). The
7 higher frequency of rapid subsidence in winter at Northern Hemisphere mid-latitudes can be
8 ascribed to the intensity of baroclinic systems, which is greatest in the wintertime. In fact, well-
9 developed tropopause folds and rapid deep intrusions are most likely to occur in the wake of
10 intense cyclogenesis, usually limited to the wintertime storm track regions (James et al., 2003).

11 Numerical models have been used to analyze ^{210}Pb and ^7Be observations at high-elevation
12 sites. 1-D model simulations of surface ^7Be showed higher concentrations at high-elevation
13 sites (Jasiulionis and Wershofen, 2005; Simon et al., 2009), but also suggested that the diffusion
14 of ^7Be was affected by the seasonal variation of meteorological conditions. Balkanski et al.
15 (1993) examined the transport of ^{210}Pb in a global 3-D model and reported a weak decrease of
16 ^{210}Pb concentrations between the continental mixed layer and the free troposphere: simulated
17 concentrations at 6-km altitude were about 50% of those in the continental mixed-layer over
18 much of the Northern Hemisphere in summer, and over large areas of the tropics year around,
19 a result consistent with the few observations available for the free troposphere at that time
20 (Moore et al., 1973). Rehfeld and Heimann (1995) compared the 3-D model simulated seasonal
21 pattern of surface ^{210}Pb and ^7Be concentrations with the observations at several sites in both
22 hemispheres. At Mauna Loa (19.47°N, 155.6°W, 3400 m asl, Hawaii) ^{210}Pb seasonality was
23 characterized by high concentrations in spring and summer and lower ones in winter, as
24 opposed to the seasonal pattern found at higher latitudes, where the ^{210}Pb maximum
25 concentrations in winter are attributed to the advective transport of ^{210}Pb aerosols from mid-

1 latitudes. This behavior is due to the elevation of the site, representative of the conditions of
2 the free troposphere rather than those of the PBL. As for ^7Be , the comparison between the
3 model and the observations at Rexburg (43.8°N, 111.83°W, 1483 m asl, USA) showed
4 systematically lower model values, due to the much higher precipitation rates in the model.

5 Previous studies have examined surface ^7Be observations at Mt. Cimone with respect to
6 the role of STE in surface ozone increases (Bonasoni et al., 1999, 2000ab; Cristofanelli et al.,
7 2003, 2006, 2009a, 2015; Lee et al., 2007) within the framework of European projects such as
8 VOTALP (Vertical Ozone Transport in the Alps) and STACCATO (influence of Stratosphere-
9 Troposphere exchange in A Changing Climate on Atmospheric Transport and Oxidation
10 capacity). These studies led to the assessment of a higher incidence of STE events during the
11 period from October to February relative to the warm season, when thermal convection and the
12 rising of the tropopause promote vertical mixing, which acts as a confounding factor in STE
13 detection. Lee et al. (2007) and Tositti et al. (2014) reported the seasonal patterns and frequency
14 distributions of ^{210}Pb and ^7Be measured at Mt. Cimone, and highlighted higher concentrations
15 of both radionuclides in the summertime due to the higher mixing height and horizontal
16 transport by regional airflows. During winter, a general increase in ^7Be is associated with a
17 decrease in ^{210}Pb , due to the dominating effect of STE and subsidence in the free troposphere.
18 At the time of this work, no model analyses of ^{210}Pb and ^7Be observations at the site have been
19 conducted.

20 In this paper, we conduct simulations of ^{210}Pb and ^7Be at Mt. Cimone with a state-of-the-
21 art global 3-D chemistry and transport model (GMI CTM) driven by assimilated
22 meteorological fields for the year of 2005. Our objectives are a better elucidation of the
23 seasonal variations of ^{210}Pb and ^7Be concentrations and an improved understanding of the roles
24 of transport and precipitation scavenging processes in their seasonalities at Mt. Cimone.

The remainder of this paper is organized as follows. Section 2 describes the measurement site, the radioactivity measurements at Mt. Cimone, and the GMI CTM. Section 3 evaluates the model performance in reproducing the observed wind and precipitation fields. Section 4 evaluates the seasonal ^{210}Pb and ^7Be concentrations in the model with those observed. Section 5 examines the sources and seasonal variations in the simulated radionuclide activities, followed by summary and conclusions in section 6.

2 Data and Methods

2.1 Radionuclide Measurements at Mt. Cimone

Mt. Cimone station (44°12' N, 10°42' E, 2165 m asl) is a global WMO-GAW station managed by the Meteorological Office of the Italian Air Force, which hosts the research platform “Ottavio Vittori” of the Institute of Atmospheric and Climate Science of the National Council of Research (ISAC-CNR). The station is located on top of the highest peak of the Italian northern Apennines, with a 360° free horizon and an elevation such that the station lies above the PBL during most of the year: the Mt. Cimone measurements are considered representative of the southern Europe/Mediterranean free troposphere (Bonasoni et al., 2000a; Fischer et al., 2003; Cristofanelli et al., 2007), although during the warmer months an influence of PBL air can be detected due both to convective processes and mountain/valley breeze regimes (Fischer et al., 2003; van Dingenen et al., 2005; Tositti et al., 2013). Note in this framework that southern Europe and Mediterranean basin are considered as a hot-spot region in terms of both climate change (e.g., Forster et al., 2007) and air quality (Monks et al., 2009), as well as a major crossroad of different air mass transport processes (Li et al., 2001; Lelieveld et al., 2002; Millàn et al., 2006; Duncan et al., 2008; Tositti et al., 2013).

At Mt. Cimone station, ^{210}Pb , ^7Be , and aerosol mass load in the form of PM_{10} have been regularly measured in the period of 1998-2011 with a Thermo-Environmental PM_{10} high-

1 volume sampler. PM₁₀ is sampled on rectangular glass fiber filters (Whatman, 20.3 cm × 25.4
2 cm, with an effective exposure area of about 407 cm²), which were manually changed every 2-
3 3 days, depending on weather conditions, failures of the sampling equipment and/or of the
4 power supply and personnel on site. The average flow rate was about 1.13 m³ min⁻¹ at standard
5 temperature and pressure (STP), with an average volume of air collected on each filter equal
6 to 3000-4000 m³ (about 48 hours of sampling, 115-175 samples per year).

7 Airborne radionuclides travel attached to particulate matters, and as a consequence of
8 their physical origin, tend to populate the fine fraction (<1.0 μm) (Winkler et al., 1998; Gaffney
9 et al., 2004). The PM₁₀ samples were subjected to non-destructive high-resolution γ-
10 spectrometry for the determination of airborne radiotracers ²¹⁰Pb and ⁷Be. The characteristics
11 of the two Hyper Pure Germanium crystal detectors (HPGe) detectors are as follows: one p-
12 type coaxial detector by Ortec/Ametek with a relative efficiency of 32.5% and FWHM 1.8 keV
13 at 1332 keV and one planar DSG detector with an active surface of 1500 mm² and FWHM 0.73
14 keV at 122 keV, for higher and lower energy ranges (100-2000 keV and 0-900 keV),
15 respectively.

16 Spectra were accumulated for at least one day to optimize peak analysis and then
17 processed with a specific software package (GammaVision-32, version 6.07, Ortec). Efficiency
18 calibration was determined on both detectors with a blank glass fiber filter traced with
19 accurately weighted aliquots of a standard solution of mixed radionuclides (QCY48,
20 Amersham) supplemented with ²¹⁰Pb, homogeneously dispersed dropwise over the filter
21 surface. Once dried under a hood under ambient conditions, the calibration filter was folded
22 into a polystyrene container in the same geometry as the unknown samples. Quantitative
23 analysis on samples was carried out by subtracting the spectrum of a blank filter in the same
24 geometry, while uncertainty on peaks (k = 1, 68% level of confidence) was calculated
25 propagating the combined error over the efficiency fit previously determined with the counting

1 error. Minimum detectable activity was calculated making use of the traditional ORTEC
2 method (ORTEC, 2003) with a peak cut-off limit of 40%. Activity data was corrected to the
3 midpoint of the time interval of collection and for the decay during spectrum acquisition. For
4 our analysis, we used monthly averages of ^{210}Pb and ^7Be data at Mt. Cimone in 2005.

5 **2.2 GMI Model**

6 The Global Modeling Initiative (GMI, <http://gmi.gsfc.nasa.gov>) is a NASA-funded
7 project aiming at improving assessments of anthropogenic perturbations to the Earth system;
8 in this framework, a CTM appropriate for stratospheric assessments was developed (Rotman
9 et al., 2001). It was firstly used to evaluate the potential effects of stratospheric aircraft on the
10 global stratosphere (Kinnison et al., 2001) and on the Antarctic lower stratosphere (Considine
11 et al., 2000). The recent version of the GMI CTM includes a full treatment of both stratospheric
12 and tropospheric photochemical and physical processes and is also capable of simulating
13 atmospheric radionuclides ^{222}Rn , ^{210}Pb , ^7Be , and ^{10}Be throughout the troposphere and
14 stratosphere (Considine et al., 2004, 2005; Rodriguez et al., 2004; Liu et al., 2016). Details of
15 the model are described in Duncan et al. (2007, 2008), Strahan et al. (2007), and Considine et
16 al. (2008).

17 In this work, we simulate ^{222}Rn , ^{210}Pb , ^7Be , and ^{10}Be using a version of the GMI model
18 with the same basic structure as described by Considine et al. (2005) and Liu et al. (2016),
19 including parameterizations of the important tropospheric physical processes such as
20 convection, wet scavenging, dry deposition and planetary boundary layer mixing.
21 Meteorological data used to drive the CTM at 2° latitude by 2.5° longitude resolution, e.g.,
22 horizontal winds, convective mass fluxes and precipitation fields, are the Modern-Era
23 Retrospective analysis for Research and Applications (MERRA) assimilated data set from the
24 NASA Global Modeling and Assimilation Office (GMAO) (Rienecker et al., 2011).

1 The flux-form semi-Lagrangian advection scheme and a convective transport algorithm
2 from the CONVTRAN routine in NCAR CCM3 physics package are used in the model. The
3 wet deposition scheme is that of Liu et al. (2001): it includes scavenging in wet convective
4 updrafts, and first-order rainout and washout from both convective anvils and large-scale
5 precipitations. The gravitational settling effect of cloud ice particles included in Liu et al.
6 (2001) is not considered here. Dry deposition of aerosols is computed using the resistance-in-
7 series approach. For the simulations of radionuclides, each simulation was run for six years,
8 recycling the MERRA meteorological data for 2005, to equilibrate the lower stratosphere as
9 well as the troposphere (Liu et al., 2001). The sixth-year output was used for analysis.

10 A uniform ^{222}Rn emission of $1.0 \text{ atom cm}^{-2} \text{ s}^{-1}$ from land under nonfreezing conditions is
11 assumed (Liu et al., 2001). Following Jacob and Prather (1990), the flux is reduced by a factor
12 of 3 under freezing conditions. The flux from oceans and ice is null. Although a large variability
13 of ^{222}Rn emission from land is observed, the above emission estimate is thought to be accurate
14 to within 25% globally (Turekian et al., 1977) and to within a factor of 2 regionally (Wilkening
15 et al., 1975; Schery et al., 1989; Graustein and Turekian, 1990; Nazaroff, 1992; Liu et al.,
16 2001).

17 Following Brost et al. (1991) and Koch et al. (1996), we used the Lal and Peters (1967)
18 ^7Be source for 1958 (solar maximum year), as it best simulated stratospheric ^7Be concentrations
19 measured from aircraft (Liu et al., 2001). The rates of ^7Be production reported more recently
20 by Usoskin and Kovaltsov (2008) broadly agree with those of Lal and Peters (1967) with
21 slightly (about 25%) lower global production rate and will be tested in a separate model study.
22 The Lal and Peters (1967) source is represented as a function of latitude and altitude (pressure)
23 and does not vary with season (see Figure 1 of Koch et al., 1996). No interannual variability in
24 the ^7Be source is considered in the model (Liu et al., 2001). This may lead to an underestimate
25 of tropospheric ^7Be concentrations, especially at high latitudes during a solar minimum (or near

1 minimum) year. Lal and Peters (1967) reported that the relative amplitude of the ^7Be production
2 rate over a 11-year solar cycle is about 13% below 300 hPa at latitudes above 45 degree.

3 Because of the coarse horizontal resolution of the model (2° latitude by 2.5° longitude),
4 the model representation of the topography at the site is poor. The elevation of Mt. Cimone in
5 the model is only 298 m, whereas in reality the mountain is 2165 m (asl) high (Figure 1). For
6 this reason, the model output was not sampled at ground level, but at the gridbox corresponding
7 to the elevation of the site. In order to see the sensitivity of model-observation comparisons to
8 spatial sampling, the model was sampled not only for the grid corresponding to the latitude and
9 longitude of Mt. Cimone, but also for the 8 adjacent grids. To better understand the sources
10 and seasonality of radiotracers in the model, we examine model output not only for ^{210}Pb , ^7Be
11 and their ratio $^7\text{Be}/^{210}\text{Pb}$ (an indicator of vertical transport [Koch et al., 1996]), which can be
12 directly compared to the measurements taken at Mt. Cimone, but also for other radiotracers and
13 quantities, e.g., ^{222}Rn , and $^{10}\text{Be}/^7\text{Be}$ (a STE tracer [Zanis et al., 2003]).

14 Year 2005 was chosen for analysis because of the availability of the observational data
15 and model output at the time of this work. As discussed later, the seasonal behavior of ^{210}Pb
16 and ^7Be radionuclides during year 2005 was “typical” for Mt. Cimone. Monthly averages of
17 ^{210}Pb and ^7Be data at Mt. Cimone were calculated for comparison with model results. To better
18 compare the seasonalities of ^{210}Pb and ^7Be between the model and the observations, the
19 monthly percentage deviations from the annual mean concentration were also calculated.

20 **3 Seasonal Variations of Transport and Precipitation at Mt. Cimone: Observations vs.** 21 **Model Simulations**

22 Mt. Cimone is the windiest meteorological station in Italy and the prevailing local winds
23 blow from S-SW and N-NE directions (Ciattaglia, 1983; Ciattaglia et al., 1987; Colombo et al.,
24 2000). The wind observations at Mt. Cimone during the period of 1998-2011, when
25 radionuclide measurements were performed at the station (Tositti et al., 2014), agree with the

1 climatology of local wind intensity and direction during the period of 1946-1999 as reported
2 by the Italian Air Force (Colombo et al., 2000). N-NE directions are more significant during
3 the cold period, and fluxes from SW are more typical of the warm period. While winds blowing
4 from the S-SW sector generate a sea air inflow, a continental air inflow is observed when winds
5 come from the N-NE sector (Ciattaglia et al., 1987).

6 However, when considering the lifetimes of ^{210}Pb (about one week) and ^7Be (about three
7 weeks) aerosols (Liu et al., 2001), it is apparent that the regional and long-range transport has
8 a much more important role than local transport. On a large scale, about 70% of background
9 air masses reaching Mt. Cimone in the period of 1996-1998 came from Atlantic and Arctic
10 areas, with a smaller contribution from the Mediterranean Basin and the eastern area, as
11 estimated by Bonasoni et al. (2000). A more recent and extended study of advection patterns
12 at Mt. Cimone (Brattich E. et al., “Advection patterns at the WMO-GAW station of Mt.
13 Cimone: seasonality, trends, and influence on atmospheric composition”, manuscript in
14 preparation, 2016), analyzing clusters of 4-day kinematic back-trajectories calculated for the
15 period of 1998-2011 with the HYSPLIT (HYbrid Single-Particle Lagrangian Integrated
16 Trajectory) model driven by the NCEP/NCAR (National Center for Environmental
17 Prediction/National Center for Atmospheric Research) meteorological reanalysis, shows that
18 the air masses advected to Mt. Cimone (55%) arrive from the Western-Atlantic-North America
19 sector, while the remaining air masses (from the Arctic, Eastern and Mediterranean Basin-
20 Northern Africa) together represent 45% of trajectories. Seasonal transport to Mt. Cimone in
21 the model is shown in Figure 2, representing winds at the elevation of Mt. Cimone (winds are
22 weaker at the model bottom layer). In agreement with the description of advection patterns at
23 the site, prevailing model winds (Figure 2) blow from the western-Atlantic sector. Slow
24 summer winds suggest the stronger influence of regional/local transport at Mt. Cimone during

1 the period (e.g., Lee et al., 2007; Marinoni et al., 2008; Tositti et al., 2013, 2014; Brattich et
2 al., 2015).

3 In the model, Mt. Cimone appears to be in a location where there is a large horizontal
4 gradient of wind (transport) during 2005. Long-range transport from Western Europe, North
5 America and Arctic region prevail during the cold period, while regional transport appears
6 more important in summer. The model is able to capture relevant features of pressure systems
7 and seasonal circulation patterns of the North Atlantic/Mediterranean/African region, such as
8 the semi-permanent high pressure system located in the North Atlantic with different positions
9 during different seasons (Bermuda/Azores high), a semi-permanent system of high pressure
10 centered in northeastern Siberia during the colder half of the year (Siberian high), and the ITCZ
11 in the summer/autumn season. However, due to the coarse resolution of the global
12 meteorological reanalysis that we use to construct the model winds, the more than 50 local-
13 scale wind systems present in the Mediterranean and surrounding regions are not resolved
14 (Burlando, 2009). In northern Europe, in fact, there are approximately two main states for the
15 atmosphere, the westerly or zonal flows modulated by the advection of Atlantic lows, and the
16 long-lived blocking anticyclonic configurations over North Sea or Scandinavia (easterly)
17 (Burlando et al., 2008).

18 In the Mediterranean region, the main cyclones during winter are essentially sub-synoptic
19 lows triggered by the major North-Atlantic synoptic systems affected by the local topography
20 of the Northern Mediterranean coast (Trigo et al., 2002), whereas in summer cyclones develop
21 because of thermal effects, orography (e.g., the Atlas Mountains), and increase in low-level
22 thermal gradients (Trigo et al., 2002; Campins et al., 2006). Again, due to the coarse resolution
23 of the meteorological data we use, these sub-synoptic processes are not resolved. For instance,
24 North-African lows and Sahara depressions (also referred to as Atlas lee depressions) and the
25 resulting S-SW wind (Sirocco) (Reiter, 1975), potentially linked to ^{210}Pb variations at Mt.

Cimone, appear to be an important feature missing in the degraded MERRA data, where they appear only during October/November. However, MERRA is able to capture the summertime north-north easterly winds in the eastern Mediterranean (Aegean Sea), known as the Etesians. The Etesians are the most persistent localized wind system in the world as a result of a sharp east–west pressure gradient manifested by large-scale circulation features (i.e., low pressure over the eastern Mediterranean/Middle East and high pressure over central and southeastern Europe) (Dafka et al., 2016).

We evaluate the MERRA precipitation with those from the GPCP (Global Precipitation Climatology Project, <http://www.gewex.org/gpcp.html>) satellite and surface observations in 2005. Figure 3 shows the MERRA and GPCP monthly precipitation for the region defined by 0–75°N and 90°W – 90°E. A good agreement between the MERRA and the GPCP precipitations averaged over the region was found. In particular, summer precipitation patterns are very similar. The geographical distribution of precipitation in MERRA shows some important features in agreement with the observed climatology precipitations: the desert climate in North Africa with very low precipitation all year long, the ITCZ with high precipitation during the summer/autumn seasons, the North Atlantic region with high precipitation especially during the winter and autumn seasons, and Europe where the seasonal pattern of precipitation is similar to that in the North Atlantic region, but precipitation is lower.

Figure 4 shows the comparison of the GPCP and MERRA precipitation seasonality at Mt. Cimone. Since Mt. Cimone is located in a region with a large horizontal gradient in precipitation, we also show in the figure the comparisons for three adjacent gridboxes. The MERRA precipitation is generally lower than that of GPCP at two gridboxes (except for summer, Figure 4ab), but in good agreement at the other two gridboxes (Figure 4cd). The agreement between the MERRA and GPCP precipitation seasonality is reasonable, with the squared correlation coefficient R^2 varying between 0.56 (at the grid to the northwest of “ij”)

Deleted: However, MERRA is able to capture the summertime north-north easterly winds in the eastern Mediterranean (Aegean Sea), known as the Etesian winds, generated by thermal effects.¶

1 and 0.89 (at the grid to the southeast of “ij”). Large differences between the MERRA
2 precipitation and that locally observed at the station are instead present. While the daily mean
3 observed 2005 precipitation is 0.81 mm, which is close to the corresponding precipitation (0.73
4 mm) in MERRA at the “ij” grid (i.e., a negative bias of -0.08 mm); the model bias is positive
5 and much higher (0.31 – 1.28 mm) at adjacent grids. This bias may very well reflect again the
6 fact that the observed surface precipitation is localized, whereas the satellite and MERRA
7 precipitations correspond to a much larger scale (about 200 km). Moreover, as Colombo et al.
8 (2000) previously pointed out, different from the surrounding area where the climate is defined
9 as temperate-continental, the climate at the mountaintop is classified as alpine because of the
10 high elevation. In fact, in agreement with the GPCP precipitation in 2005, the observed
11 climatology in the region shows maximum during November (secondary maximum in spring)
12 and absolute minimum in July (secondary minimum in January), whereas on the top of the
13 mountain the precipitation is maximal during summer. The MERRA precipitation shows
14 increased amounts during April and August-December, with minimum in June-July. As the
15 local precipitation at the site is important to the scavenging of radionuclide aerosol tracers, this
16 difference between the local and regional precipitation could contribute to any biases in our
17 simulations. However, as we will show below, the ratio $^7\text{Be}/^{210}\text{Pb}$ may cancel out the errors
18 associated to precipitation scavenging (Koch et al., 1996).

19 Low ^{210}Pb concentrations are seen over the Atlantic Ocean, due to the negligible
20 emissions of ^{222}Rn from the oceans and strong precipitation scavenging, and in northern and
21 western Europe especially during the cold season (Figure 2a). High ^{210}Pb concentrations appear
22 over the Sahara Desert and North Africa, as a result of low precipitation in this area, and also
23 over the Middle East and South Asia. ^{210}Pb concentrations over southern Europe appear higher
24 during the transition seasons, especially fall, and peak during summer when the minimum
25 precipitation and slow winds from west are observed in the region. Low ^7Be concentrations are

Formatted: Font color: Red

1 simulated along the equator where convective scavenging is strongest (Figure 2b). High ^7Be
2 concentrations are seen over the Sahara Desert due to a combination of low precipitation and
3 subsidence in this region. Elevated values also occur over the Middle East, North America, and
4 Greenland. ^7Be concentrations over southern Europe appear higher during spring and peak
5 during winter, when model winds are stronger and transport ^7Be aerosols from North America
6 and Greenland regions where ^7Be production is highest (Beer et al., 2012).

7 **4 Seasonal Variations of ^{210}Pb and ^7Be at Mt. Cimone: Observations vs. Model** 8 **Simulations**

9 The seasonality and frequency distributions of ^{210}Pb and ^7Be concentrations measured at
10 the Mt. Cimone station were previously examined by Lee et al. (2007), while more recent
11 analyses of the 12-year record were presented in Tositti et al. (2014) and Brattich et al. (2015).
12 Generally, both radionuclides show a marked seasonal maximum in the summertime, a
13 behaviour shared by PM_{10} (Tositti et al., 2013) and O_3 (Bonasoni et al., 2000b). ^{210}Pb summer
14 maximum is mainly due to the higher mixing height and enhanced uplift from the boundary
15 layer as a result of thermal convection. The seasonal fluctuation of ^7Be is more complex and
16 characterized by two relative maxima, one during the cold season associated with stratosphere-
17 to-troposphere transport, and the other during the warm season mainly associated with
18 tropospheric subsidence balancing lower-tropospheric air masses ascent occasionally
19 accompanied by STE (Tositti et al., 2014). The ^{210}Pb and ^7Be measurements in 2005 are
20 consistent with this description (Figure 5): ^{210}Pb concentrations are characterized by two
21 maxima during the warm period (July and September); ^7Be concentrations are characterized by
22 one absolute maximum during summer (July) and one secondary maximum during spring
23 (March).

24 Figure 5 (ab) compares the simulated monthly ^{210}Pb and ^7Be activities with the
25 observations at Mt. Cimone in 2005. The comparisons for the monthly percentage deviations

from the annual mean concentration are available as Supplementary Information (hereafter SI, SI Figures 1-2). The seasonality of ^{210}Pb is well captured by the model. The model reproduces the presence of two seasonal maxima in the ^{210}Pb observations, with the maximum observed in July shifted to June in the simulation. The squared correlation coefficient R^2 between observed and simulated ^{210}Pb activities is equal to 0.83 at the “ij” grid and varies between 0.42 and 0.82 for adjacent gridboxes (to the north and to the west of “ij”, respectively), confirming the good performance of the model in reproducing the ^{210}Pb seasonal pattern.

As for ^7Be , the model well captures the March maximum (i.e., secondary maximum in the observations) and the month-to-month variation during the cold and transition seasons (January-April, October-December). However, during the warm period, the simulated ^7Be concentrations are lower by a factor of 2 than the observed. A better agreement was found at some adjacent model gridboxes (e.g., to the south and to the southwest of “ij”; Figure 6 vs. Figure 5). The correlation between observed and simulated monthly ^7Be activities also increases from $R^2 = 0.03$ at “ij” to $R^2 = 0.11$ - 0.60 at adjacent model gridboxes. The largest value of $R^2 = 0.6$ was obtained at the “ij-1” gridbox to the south of “ij” (Figure 6). This improvement is due to the large horizontal gradient in the simulated ^7Be concentrations near the site (Figure 2).

5 Sources and Seasonality of ^{210}Pb and ^7Be at Mt. Cimone: A Model Analysis

In this section, we quantify the sources of ^{210}Pb and ^7Be and determine the processes governing their seasonality in the GMI model. Additional tracers as simulated by the model are used to aid in the interpretation. Model sensitivity experiments are conducted to examine the roles of transport and precipitation scavenging in the seasonality.

As discussed in Section 4, the model well reproduces the ^{210}Pb seasonality, with minimum in the cold period and maximum in the warm period. The ^{210}Pb seasonality (Figure

1 5a) can be linked with the seasonal pattern of its precursor ^{222}Rn (Figure 5c). It is seen that the
2 summer ^{210}Pb maximum is due to stronger (thermal) convection, which uplifts more ^{222}Rn out
3 of the boundary layer (e.g., Lee et al., 2007; Tositti et al., 2014; Brattich et al., 2015). This
4 uplift of ^{222}Rn from the boundary layer is minimum in the cold period, and the minimal level
5 of ^{210}Pb in this period can be considered representative of the free troposphere. The ^{210}Pb
6 summer increase appears to be associated with short-range and regional transport, as suggested
7 by the model simulations (Figure 2a). As expected, long-range transport is more typical of the
8 winter/spring seasons because of stronger horizontal winds, while regional effects are more
9 important during summer when convection gets stronger.

10 In a similar manner, the source of the ^7Be March maximum can be investigated with
11 model tracer simulations. Figure 5 (de) also shows the simulated seasonal patterns of the
12 $^{10}\text{Be}/^7\text{Be}$ activity ratio and of the fraction of ^7Be originating from the stratosphere (strat
13 $^7\text{Be}/\text{total } ^7\text{Be}$). The simulated seasonal pattern of the $^{10}\text{Be}/^7\text{Be}$ ratio is very similar to the
14 observations at Jungfraujoch (Switzerland, 3580 m asl) (Zanis et al., 2003), characterized by a
15 clear seasonal cycle with peak ratios in spring. The usefulness of $^{10}\text{Be}/^7\text{Be}$ ratio as a
16 stratospheric tracer is due to the fact that both ^{10}Be and ^7Be cosmogenic radionuclides attach
17 to the same aerosols and share therefore the same removal mechanism. Moreover, due to the
18 much longer physical half-life of ^{10}Be ($\tau_{1/2} = 1.5 \times 10^6$ years) compared to ^7Be ($\tau_{1/2} = 53.3$
19 days), their concentration ratios in the stratosphere (about 3–4) are much higher than in the
20 troposphere (about 2 or even less) (Koch and Rind, 1998). The simulated $^{10}\text{Be}/^7\text{Be}$ ratio
21 behavior indicates that deep stratosphere-to-troposphere (STT) peaks during winter, while
22 shallower STT has a spring maximum, consistent with previous analyses of stratospheric
23 intrusions at Mt. Cimone (Cristofanelli et al., 2006, 2009), and more generally with the
24 climatology of stratosphere-troposphere exchange at the Northern Hemisphere mid-latitudes
25 (James et al., 2003). Altogether the simulated high strat $^7\text{Be}/\text{total } ^7\text{Be}$, high $^7\text{Be}/^{210}\text{Pb}$ (Figure

7), and low $^{10}\text{Be}/^7\text{Be}$ ratios during December-January indicate strongest STE during this period, followed by spring with slightly weaker stratospheric influence on surface ^7Be . However, the model tends to overestimate the observed ^7Be concentrations and $^7\text{Be}/^{210}\text{Pb}$ ratios during December-February, suggesting that stratospheric influence and/or subsidence in the model is probably too strong in this region at this time of the year. It is noted that globally integrated STT mass fluxes in the MERRA reanalysis are actually smaller than in some other reanalyses, e.g., ERA-Interim, JRA-55, and MERRA-2 (Boothe and Homeyer, 2016).

The use of the ^7Be production rate of Lal and Peters (1967) for a solar maximum year (1958) may partly explain the lower annual mean ^7Be in the model (3.4 mBq m^{-3} annual mean at the “ij” grid) than in the observations (4.2 mBq m^{-3}). In fact, the sunspot number in 2005 (29.8) was quite low (slowly decreasing from 2000, a solar maximum year, and reaching minimum in 2008), especially compared to the 1958 value of 184.8. Sunspot number data are available from the World Data Center for the production, preservation and dissemination of the international sunspot number (Sunspot Index and Long-term Solar Observation, SILSO, Royal Observatory of Belgium, Brussels, <http://sidc.oma.be/sunspot-data/>).

During the winter period, associated with the simulated and observed ^7Be increases (Figures 5-6), strong long-range transport was dominant in the European region (Figure 2b). Transport from higher latitude regions (Arctic, northern Europe, and North America) appears particularly important during this period (Figure 2b); such transport from high-latitude regions, where the ^7Be production rate is highest (Beer et al., 2012), has typically been observed during STE events at Mt. Cimone in many studies (e.g., Bonasoni et al., 1999, 2000ab).

The discrepancy between the simulated and the observed ^7Be concentrations during the warm period is partly due to the sensitivity to spatial sampling in the model. As seen from the map plots of ^{210}Pb and ^7Be concentrations at the elevation of Mt. Cimone (Figure 2), the sampling site appears to be located in a region where the N-S gradient of concentrations is large

1 (especially for ^7Be). An elevated gradient in the region surrounding Mt. Cimone was also seen
2 for winds, as transport plays a critical role in determining the distributions of these tracers. The
3 sensitivity to spatial sampling in the model is therefore ascribed to this observed strong gradient
4 in the N-S direction. In fact, while the grids to the south and southwest of “ij” are better for
5 summer ^7Be comparisons (Figure 6), the grids to the northeast, north, and northwest of “ij” are
6 better for winter (not shown).

7 The model underestimate of ^7Be levels in the warm months may also suggest the mixing
8 of air masses between the PBL and the lower free troposphere is likely too weak. Previous
9 observational analyses indicated that such mixing is higher in summer at Mt. Cimone due to
10 enhanced convection and mountain wind breeze (e.g., Fischer et al., 2003; Cristofanelli et al.,
11 2007). Weaker entrainment of free-tropospheric air into the PBL would result in lower ^7Be
12 concentrations at the surface.

13 The model annual average biases are about 8% for ^{210}Pb and about 19% for ^7Be ,
14 respectively. By contrast, the model average bias for $^7\text{Be}/^{210}\text{Pb}$ ratios is about -13% (Figure 7).
15 The smaller model bias for $^7\text{Be}/^{210}\text{Pb}$ ratios than for ^7Be concentrations reflects the fact that the
16 ratio cancels out the errors in precipitation scavenging (Koch et al. 1996) that contribute to the
17 underestimate of ^{210}Pb and ^7Be activities. On the other hand, the negative model bias for the
18 $^7\text{Be}/^{210}\text{Pb}$ ratio again points to weak downward mixing from the free troposphere.

19 If one compares the month-to-month variation of ^{210}Pb and ^7Be (Figures 5 and 6) and
20 precipitation in the model (Figure 4), the maxima/minima of precipitation appear to be in phase
21 with those of both radionuclides' activities. This reflects the effects of precipitation scavenging
22 on radionuclide aerosols.

23 We conducted model sensitivity experiments where convection (transport and
24 scavenging), wet scavenging due to both large-scale and convective precipitation, and dry
25 deposition processes are turned off, respectively, to examine the roles of these processes in

1 controlling the seasonality of ^{210}Pb and ^7Be at Mt. Cimone. Figure 8 shows the results for the
2 standard and sensitivity runs at the “grid to the south of “ij”, for which the simulated tracer
3 seasonal variations are similar to those observed, while the monthly percentage deviations from
4 the annual mean concentrations are shown in SI Figure 3. Figures 9-12 show maps of simulated
5 changes in ^{210}Pb and ^7Be concentrations when convection or wet scavenging is turned off.

6 Turning off dry deposition does not significantly change the simulated ^{210}Pb and ^7Be
7 concentrations, partly due to sampling the higher vertical gridbox in the model (larger effects
8 are seen at the bottom model layer). Turning off convection (i.e., with neither convective
9 transport nor convective scavenging), the simulated ^7Be seasonality also remains nearly the
10 same. This suggests the compensating effects between subsidence (increasing ^7Be) associated
11 with convective transport and scavenging (decreasing ^7Be) due to convective precipitation. In
12 the case of ^{210}Pb , turning off convection does not change the seasonal pattern but generally
13 results in larger ^{210}Pb concentrations and particularly during summer/autumn when convective
14 transport is more important at the site. In fact, no convective transport of ^{222}Rn (SI Figure 5)
15 results in less ^{222}Rn (and ^{210}Pb) being transported to the free troposphere, but also more ^{210}Pb
16 available in PBL lifted to the free troposphere by large-scale vertical transport; on the other
17 hand, lack of convective scavenging of ^{210}Pb increases its concentration in the free troposphere.
18 Turning off convection therefore results in an increase of ^{210}Pb concentrations in the free
19 troposphere. Both surface ^{222}Rn concentrations at the elevation of Mt. Cimone (SI Figure 4),
20 as well as a map of changes in ^{210}Pb concentrations due to convection in the model (Figure 9)
21 show that convection in the region is more important during summer and autumn, but is not
22 negligible during spring, possibly due to thermal inertia.

23 The model run without scavenging suggests that, apart from downward transport from
24 the upper troposphere and lower stratosphere, wet scavenging is mainly responsible for the
25 seasonal variation of ^7Be (Figure 8, bottom panel). None of our simulations is able to describe

1 the observed ^7Be summertime peak, suggesting that local and regional circulations in this
2 region with complex topography may not be resolved by the coarse-resolution model. For ^{210}Pb
3 (Figure 8, top panel), it appears that wet scavenging plays a more important role during August-
4 December than during January-July. This appears to be associated with the seasonality of
5 precipitation, which shows prolonged elevated values during August-December, as well as a
6 maximum during April, as previously discussed (Figure 5). A plot of changes in ^{210}Pb
7 concentrations due to scavenging in the model (Figure 10) confirms that the scavenging effect
8 is larger during fall and, to a lesser extent, during summer. At Mt. Cimone, the scavenging
9 effect is not minimal during July (month of minimum precipitation, Figure 4), suggesting the
10 influence of precipitation scavenging elsewhere in the region on the site.

11 **6 Summary and Conclusions**

12 We have used a global 3-D model (GMI CTM) driven by the MERRA assimilated
13 meteorological data from NASA's GMAO to simulate the ^{210}Pb and ^7Be observations from the
14 Mt. Cimone (44°12' N, 10°42' E, 2165 m asl, Italy) WMO-GAW station in 2005. The two
15 natural atmospheric radionuclides originate from contrasting source regions (lower troposphere
16 and upper troposphere/lower stratosphere, respectively), attach to submicron particles, and are
17 removed from the troposphere mainly by wet deposition. Our objective was to examine the
18 roles of horizontal advection, vertical transport (large-scale and convection), and wet
19 scavenging in determining the seasonality of ^{210}Pb and ^7Be at Mt. Cimone. The observed ^{210}Pb
20 concentrations are characterized by maxima in summer and minima during the cold period.
21 The seasonality of ^7Be is more complex, with a major peak in summer, a secondary peak in
22 spring and a minimum in winter. This is the first modeling study of ^{210}Pb and ^7Be observations
23 at Mt. Cimone. This site is representative of free-tropospheric Southern Europe/Mediterranean
24 conditions most of the year, and as such the comparison between measurements and

1 simulations can serve as an indication of shortcomings in the model or in the meteorological
2 data.

3 Precipitation and wind fields are important to the model's performance in representing
4 the transport and scavenging processes. We evaluated the MERRA precipitation field used by
5 GMI CTM against the GPCP satellite and surface observations, and a generally good
6 agreement was found. The seasonality of precipitation at Mt. Cimone shows increased amounts
7 during April and the period of August-December, and minimum in June-July. The MERRA
8 assimilated winds at the low-resolution version we used captured the main circulation patterns
9 (e.g., location of the Azores high pressure, location of the ITCZ) in the Northern Hemisphere.
10 However, some local-scale winds and pressure systems, which are important for transport to
11 the sampling site, were likely not well resolved at the coarse resolution we used. A general
12 good agreement was found between the MERRA assimilated wind fields and the main
13 advection patterns at the site (e.g., prevalence of long-range transport from Western Europe,
14 North America and Arctic region during the cold season, as opposed to the prevailing regional
15 transport during the warm season).

16 The model well reproduced the observed ^{210}Pb seasonality: ^{210}Pb maxima during the
17 warm period were attributed to the stronger (thermal) convection, which uplifts more ^{222}Rn
18 (and ^{210}Pb) from the boundary layer. The model is less successful in reproducing the observed
19 ^7Be seasonality. ^7Be was better represented during the cold period, while the observed summer
20 ^7Be maximum was underestimated by the model. The model underestimate of ^7Be levels in the
21 warm months is partly due to the sensitivity to spatial sampling in the model, but also suggests
22 that the mixing of air masses between the PBL and the lower free troposphere (e.g., via
23 convection and compensating subsidence) is likely too weak during summer when the Mt.
24 Cimone station is located within the PBL. This suggests that additional work comparing the
25 model results with more surface observations is needed in order to better understand this effect.

1 The simulated lower annual average ^7Be concentration relative to the observation is also partly
2 attributed to the fact that the model used the ^7Be production rate for a solar maximum year,
3 while in 2005 (our simulation year) the solar activity was rather low.

4 By examining the wind fields and horizontal distribution of radiotracers in the model, we
5 noted that the sampling site is in a location where there is a large gradient, especially in the
6 North-South direction. Accordingly, we investigated the sensitivity of model results to spatial
7 sampling. A better agreement between the model and the observations at some adjacent
8 gridboxes was found. The ^7Be March maximum was linked to the large stratospheric influence
9 during winter/spring. The model tends to underestimate the summertime ^{210}Pb and ^7Be , but
10 better simulates the $^7\text{Be}/^{210}\text{Pb}$ ratio because the model errors due to precipitation scavenging
11 appear to be canceled out in the ratio.

12 We have conducted a series of model sensitivity experiments to further examine and
13 quantify the roles of wet scavenging, dry deposition, and convection (transport and scavenging)
14 in controlling the seasonality of ^{210}Pb and ^7Be at Mt. Cimone. Dry deposition does not have a
15 significant effect on the magnitude and seasonality of ^{210}Pb and ^7Be concentrations at the site.
16 The relatively weak combined effects of convective transport and convective scavenging on
17 the radiotracer seasonality were attributed to the compensating effects of convective transport
18 and convective scavenging on tracer concentrations in the lower free troposphere (at the
19 elevation of Mt. Cimone). Convection appears to be more important to the regional distribution
20 of both radiotracers during summer and autumn, although it is also significant during spring.
21 Finally, scavenging is found to be the most important process controlling the seasonal
22 variations of ^{210}Pb and ^7Be at Mt. Cimone. For ^{210}Pb , precipitation plays a more important role
23 during August-December than during January-July. This was attributed to the seasonality of
24 local and regional precipitation, which shows prolonged elevated values in the period of
25 August-December.

1 While our simulations demonstrated some capabilities of the model to reproduce the
2 seasonality of ^{210}Pb and ^7Be , they highlight the weaknesses of the model in reproducing local
3 features, presumably due to its coarse resolution. Model simulations at a higher resolution
4 would improve this model analysis of ^{210}Pb and ^7Be observations at Mt. Cimone, a high-
5 elevation site. The understanding of downward transport associated with convection during
6 summer also requires improving. As such, ^{210}Pb and ^7Be tracers will prove to be very useful in
7 our understanding of seasonal behaviors of other environmentally important trace gases and
8 aerosols at Mt. Cimone. Since other aerosols and trace gases (e.g., black carbon, CO, O₃) are
9 also measured at the station, we plan to conduct comparisons between model simulations and
10 those measurements to corroborate or contrast with the radionuclide results.

12 **Data availability**

13 A description of the observational data and model output used in this paper can be found in
14 Sect. 2 and they are available upon request by contacting Laura Tositti (laura.tositti@unibo.it)
15 and Hongyu Liu (hongyu.liu-1@nasa.gov), respectively.

17 **Acknowledgements.** Italian Air Force Meteorological Office (IAFMS) and ISAC-CNR are
18 gratefully acknowledged for their precious technical support at the Mt. Cimone station. In
19 particular, ISAC-CNR is gratefully acknowledged for providing infrastructural access at the
20 WMO-GAW Global Station Italian Climate Observatory "O. Vittori" at Mt. Cimone. IAFMS
21 is gratefully acknowledged for providing meteorological observations at Mt. Cimone station.
22 The Italian Climate Observatory "O. Vittori" is supported by MIUR and DTA-CNR throughout
23 the Project of National Interest NextData. Erika Brattich thanks the National Institute of
24 Aerospace (NIA) Visitor Program for hosting her one month visit, and the Department of
25 Biological, Geological and Earth Sciences of the University of Bologna for grant support

1 during her PhD study. Hongyu Liu is supported by NASA Modeling and Analysis Program
2 (MAP), NASA Atmospheric Composition Modeling and Analysis Program (ACMAP), and
3 NASA Atmospheric Composition Campaign Data Analysis and Modeling (ACCDAM)
4 program. The GMI activity is managed by José Rodriguez and Susan Strahan (NASA GSFC).
5 Stephen Steenrod, Megan Damon, and Jules Kouatchou (GSFC) are acknowledged for
6 programming support. NASA Center for Computational Sciences (NCCS) provided
7 supercomputing resources.

8

9 **References**

- 10 Arimoto, R., Snow, J.A., Graustein, W.C., Moody, J.L., Ray, B.J., Duce, R.A., Turekian, K.K.,
11 and Maring H.B.: Influences of atmospheric transport pathways on radionuclide activities
12 in aerosol particles from over the North Atlantic, *J Geophys Res*, 104(D17), 301-321, 1999.
- 13 Balkanski, Y, Jacob, D.J., Gardner, G.M., Graustein, W., Turekian, K.K.: Transport and
14 residence times of tropospheric aerosols inferred from a global three-dimensional
15 simulation of ^{210}Pb , *J Geophys Res*, 98 (D11), 20573-20586, 1993.
- 16 Baskaran, M.: Po-210 and Pb-210 as atmospheric tracers and global atmospheric Pb-210
17 fallout: a review, *J Environ Radioactiv*, 102, 500-513, 2011.
- 18 Beer, J., McCracken, K., and von Steiger, R.: *Cosmogenic radionuclides*. Springer, Heidelberg,
19 Germany, 2012.
- 20 Bonasoni, P., Evangelisti, F., Bonafé, U., Feldmann, H., Memmesheimer, M., Stohl, A., and
21 Tositti, L.: Stratosphere-troposphere exchanges: case studies recorded at Mt. Cimone
22 during VOTALP project, *Phys Chem Earth (C)*, 24(5), 443-446, 1999.
- 23 Bonasoni, P., Evangelisti, F., Bonafé, U., Ravegnani, F., Calzolari, F., Stohl, A., Tositti, L.,
24 Tubertini, O., and Colombo, T.: Stratospheric ozone intrusion episodes recorded at Mt.
25 Cimone during VOTALP project: Case studies, *Atmos Environ*, 34, 1355-1365, 2000a.

1 Bonasoni, P., Stohl, A., Cristofanelli, P., Calzolari, F., Colombo, T., and Evangelisti, F.:
2 Background ozone variations at Mt Cimone station, *Atmos Environ*, 34, 5183-5189, 2000b.

3 Boothe, A. C. and Homeyer, C. R.: Global large-scale stratosphere-troposphere exchange in
4 modern reanalyses, *Atmos. Chem. Phys. Discuss.*, doi:10.5194/acp-2016-788, in review,
5 2016.

6 Bourcier, L., Masson, O., Laj, P., Pichon, J.M., Paulat, P., Freney, E., and Sellegri, K.:
7 Comparative trends and seasonal variation of ^7Be , ^{210}Pb and ^{137}Cs at two altitude sites in
8 the central part of France, *J Environ Radioactiv*, 102, 294-301, 2011.

9 Brattich, E., Hernández-Ceballos, M.A., Cinelli, G., and Tositti, L.: Analysis of peak ^{210}Pb
10 values at Mt. Cimone (1998-2011), *Atmos Environ*, 112, 136-147, 2015.

11 Brattich, E., Orza, J.A.G., and Tositti, L.: Advection patterns at the WMO-GAW station of Mt.
12 Cimone: seasonality, trends, and influence on atmospheric composition, manuscript in
13 preparation, 2016.

14 Brost, R.A., Feichter, J., and Heimann, H.: Three-dimensional simulation of ^7Be in a global
15 climate model, *J Geophys Res*, 96, 22423-22445, 1991.

16 Burlando, M.: The synoptic-scale surface wind climate regimes of the Mediterranean Sea
17 according to the cluster analysis of ERA-40 wind fields, *Theor Appl Climatol*, 96, 69-83,
18 2009.

19 Burlando, M., Antonelli, M., and Ratto, C.F.: Mesoscale wind climate analysis: identification
20 of anemological regions and wind regimes, *Int J Climatol*, 28, 629-641, 2008.

21 Caillet, S., Arpagaus, P., Monna, F., and Dominik, J.: Factors controlling ^7Be and ^{210}Pb
22 atmospheric deposition as revealed by sampling individual rain events in the region of
23 Geneva, Switzerland, *J Environ Radioactiv*, 53, 241-256, 2001.

24 Campins, J., Jansà, A., and Genovés, A.: Three-dimensional structure of western
25 Mediterranean cyclones, *Int J Climatol*, 26, 323-343, 2006.

1 Cannizzaro, F., Greco, G., Raneli, M., Spitale, M.C., and Tomarchio, E.: Concentration
2 measurements of ^7Be at ground level air at Palermo, Italy – comparison with solar activity
3 over a period of 21 years, *J Environ Radioactiv*, 84, 457-467, 2004.

4 Carvalho, A.C., Reis, M., Silva, L., and Madruga, M.J.: A decade of ^7Be and ^{210}Pb activity in
5 surface aerosols measured over the Western Iberian Peninsula, *Atmos Environ*, 67, 193-
6 202, 2013.

7 Ciattaglia, L.: Interpretation of atmospheric CO_2 measurements at Mt. Cimone (Italy) related
8 to wind data. *Journal of Geophysical Research* 88, C2, 1331-1338, 1983.

9 Ciattaglia, L., Cundari, V., and Colombo, T.: Further measurements of atmospheric carbon
10 dioxide at Mt. Cimone, Italy: 1979-1985, *Tellus B*, 39, 13-20, 1987.

11 Colombo, T., Santaguida, R., Capasso, A., Calzolari, F., Evangelisti, F., and Bonasoni, P.:
12 Biospheric influence on carbon dioxide measurements in Italy, *Atmos Environ*, 34, 4963-
13 4969, 2000.

14 Considine, D.B., Douglass, A.R., Connell, P.S., Kinnison, D.E., and Rotman, D.A.: A polar
15 stratospheric cloud parameterization for the global modeling initiative three-dimensional
16 model and its response to stratospheric aircraft, *J Geophys Res*, 105(D3), 3955-3973, 2000.

17 Considine, D.B., Connell, P.S., Logan, J.A.: Simulating ozone in the near tropopause region
18 with a new combined model of the stratosphere and troposphere, in: *Quadrennial Ozone*
19 *Symposium QOS 2004*, edited by: Zerefos, C, International Ozone Commission, Kos,
20 Greece, pp. 739-740, 2004.

21 Considine, D.B., Bergmann, D.J., and Liu, H.: Sensitivity of Global Modeling Initiative
22 chemistry and transport model simulations of radon-222 and lead-210 to input
23 meteorological data, *Atmos Chem Phys*, 5, 3389-3406, 2005.

24 Cristofanelli, P., Bonasoni, P., Collins, W., Feichter, J., Forster, C., James, P., Kentarchos, A.,
25 Kubik, P.W., Land, C., Meloen, J., Roelofs, G.J., Siegmund, P., Sprenger, M., Schnabel,

1 C., Stohl, A., Tobler, L., Tositti, L., Trickl, T., and Zanis, P.: Stratosphere-to-troposphere
2 transport: A model and method evaluation, *J Geophys Res*, 108(D12), 8525,
3 doi:10.1029/2002JD002600, 2003.

4 Cristofanelli, P., Bonasoni, P., Tositti, L., Bonafé, U., Calzolari, F., Evangelisti, F., Sandrini,
5 S., and Stohl, A.: A 6-year analysis of stratospheric intrusions and their influence on ozone
6 at Mt. Cimone (2165 m above sea level), *J Geophys Res*, 111, D03306,
7 doi:10.1029/2005JD006553, 2006.

8 Cristofanelli, P., Bonasoni, P., Carboni, G., Calzolari, F., Casarola, L., Zauli Sajani, S., and
9 Santaguida, R.: Anomalous high ozone concentrations recorded at a high mountain station
10 in Italy in summer 2003, *Atmos Environ*, 41, 1383-1394, 2007.

11 Cristofanelli, P., Calzolari, F., Bonafé, U., Duchi, R., Marinoni, A., Roccato, F., Tositti, L., and
12 Bonasoni P.: Stratospheric intrusion index (SI²) from baseline measurement data, *Theor*
13 *Appl Climatol*, 97, 317-325, 2009a.

14 Cristofanelli, P., Marinoni, A., Arduini, J., Bonafé, U., Calzolari, F., Colombo, T., Decesari,
15 S., Duchi, R., Facchini, M.C., Fierli, F., Finessi, E., Maione, M., Chiari, M., Calzolari, G.,
16 Messina, P., Orlandi, E., Roccato, F., and Bonasoni, P.: Significant variations of trace gas
17 composition and aerosol properties at Mt. Cimone during air mass transport from North
18 Africa – contributions from wildfire emissions and mineral dust, *Atmos Chem Phys*, 9,
19 4603-4619, 2009b.

20 Cristofanelli, P., Scheel, H.-E., Steinbacher, M., Saliba, M., Azzopardi, F., Ellul, R., Fröhlich,
21 M., Tositti, L., Brattich, E., Maione, M., Calzolari, F., Duchi, R., Landi, T.C., Marinoni,
22 A., and Bonasoni, P.: Long-term surface ozone variability at Mt. Cimone WMO/GAW
23 global station (2165 m a.s.l., Italy), *Atmos Environ*, 101, 23-33, 2015.

1 Cuevas, E., Gonzalez, Y., Rodríguez, S., Guerra, J.C., Gómez-Peláez, A.J., Alonso-Pérez, S.,
2 Bustos, J., and Milford, C.: Assessment of atmospheric processes driving ozone variations
3 in the subtropical North Atlantic free troposphere, *Atmos Chem Phys*, 13, 1973-1998, 2013.

4 [Dafka, S., Xoplaki, E., Toreti, A., Zanis, P., Tyrlis, E., Zerefos, C., and Luterbacher,](#)
5 [J., 2016: The Etesians: from observations to reanalysis. *Clim. Dyn.*, 47, 1569-1585.](#)
6 [doi:10.1007/s00382-015-2920-7.](#)

7 Daish, S.R., Dale, A.A., Dale, C.J., May, R., and Rowe, J.E.: The temporal variations of ^7Be ,
8 ^{210}Pb and ^{210}Po in England, *J Environ Radioactiv*, 84, 457-467, 2005.

9 Dibb, J.E., Talbot, R.W., and Gregory, G.L.: Beryllium 7 and lead 210 in the western
10 hemisphere Arctic atmosphere: Observations from three recent aircraft-based sampling
11 programs, *J Geophys Res*, 97, 16709-16715, 1992.

12 Dibb, J.E., Meeker, L.D., Finkel, R.C., Southon, J.R., Caffee, M.W., and Barrie, L.A.:
13 Estimation of stratospheric input to the Arctic troposphere: ^7Be and ^{10}Be in aerosols at
14 Alert, Canada, *J Geophys Res*, 99, 12855-12864, 1994.

15 Dibb, J.E.: Vertical mixing above Summit, Greenland: insights into seasonal and high
16 frequency variability from the radionuclide tracers ^7Be and ^{210}Pb , *Atmos Environ*, 41, 5020-
17 5030, 2007.

18 Dueñas, C., Fernández, M.C., Cañete, S., and Pérez, M.: ^7Be to ^{210}Pb concentration ratio in
19 ground level air in Málaga (36.7°N, 4.5°W), *Atmos Res*, 92, 49-57, 2009.

20 Dueñas, C., Orza, J.A.G., Cabello, M., Fernández, M.C., Cañete, S., Pérez, M., and Gordo, E.:
21 Air mass origin and its influence on radionuclide activities (^7Be and ^{210}Pb) in aerosol
22 particles at a coastal site in the western Mediterranean, *Atmos Res*, 101, 205-214, 2011.

23 Duncan, B.N., Strahan, S.E., and Yoshida, Y.: Model study of the cross-tropopause transport
24 of biomass burning pollution, *Atmos Chem Phys*, 7, 3713-3736, 2007.

1 Duncan, B.N., West, J.J., Yoshida, Y., Fiore, A.M., and Ziemke, J.R.: The influence of
2 European pollution on ozone in the Near East and northern Africa, *Atmos Chem Phys*, 8,
3 2267-2283, doi:10.5194/acp-8-2267-2008, 2008.

4 Feely, H.W., Larsen, R.J., and Sanderson, C.G.: Factors that cause seasonal variations in
5 beryllium-7 concentrations in surface air, *J Environ Radioactiv*, 9, 223-249, 1989.

6 Feichter, J., Brost, R.A., and Heimann, M.: Three-dimensional modeling of the concentration
7 and deposition of ²¹⁰Pb aerosols, *J. Geophys. Res.*, 96, 22 447-22 469, 1991.

8 Fischer, H., Kormann, R., Klüpfel, T., Gurk, C., Königstedt, R., Parchatka, U., Mühle, J., Rhee,
9 T.S., Brenninkmeijer, C.A.M., Bonasoni, P., and Stohl, A.: Ozone production and trace gas
10 correlations during the June 2000 MINATROC intensive measurement campaign at Mt.
11 Cimone. *Atmos Chem Phys*, 3, 725-738, 2003.

12 Forster, P., Ramaswamy, V., Artaxo, P., Berntsen, T., Betts, R., Fahey, D.W., Haywood, J.,
13 Lean, J., Lowe, D.C., Myhre, G., Nganga, J., Prinn, R., Raga, G., Schulz, M., and Van
14 Dorland, R.: Changes in Atmospheric Constituents and in Radiative Forcing, in *Climate*
15 *Change 2007: The Physical Science Basis. Contribution of Working Group I to the Fourth*
16 *Assessment Report of the Intergovernmental Panel on Climate Change*, [Solomon, S., Qin,
17 D., Manning, M., Chen, Z., Marquis, M., Averyt, K.B., Tignor, M., and Miller, H.L. (eds.)],
18 Cambridge University Press, Cambridge, United Kingdom and New York, NY, USA, 2007.

19 Froehlich, K., and Masarik, J.: Radionuclides as tracers and timers of processes in the
20 continental environment – Basic concepts and methodologies. In: *Radioactivity in the*
21 *Environment*, 16, Chapter 2, 27-50, *Environmental Radionuclides: Tracers and Timers of*
22 *Terrestrial Processes*. Edited by Elsevier. doi:10.1016/S1569-4860(09)01602-7, 2010

23 Gaffney, J.S, Marley, N., and Cunningham, M.M.: Natural radionuclides in fine aerosols in the
24 Pittsburgh area, *Atmos Environ*, 38, 3191-3200, 2004.

25 Gäggeler, H.W.: Radioactivity in the atmosphere, *Radiochim Acta*, 70-71, 345-353, 1995.

1 Gerasopoulos, E., Zanis, P., Stohl, A., Zerefos, C.S., Papastefanou, C., Ringer, W., Tobler, L.,
2 Hübener, S., Gägger, H.W., Kanter, H.J., Tositti L., and Sandrini, S.: A climatology of
3 ^7Be at four high-altitude stations at the Alps and the Northern Apennines, *Atmos Environ*,
4 35, 6347-6360, 2001.

5 Gerasopoulos, E., Zanis, P., Zerefos, C.S., Papastefanou, C., Ringer, W., Gägger, H.W.,
6 Tobler, L., and Kanter, H.J.: Factors and processes controlling the concentration of the
7 cosmogenic radionuclide ^7Be at high-altitude Alpine stations, In: *Radioactivity in the*
8 *Environment*, Volume 7, 863-870, Elsevier Ltd., ISSN 1569-4860, DOI10.1016/S1569-
9 4860(04)07108-6, 2005.

10 Graustein, W.C., and Turekian, K.K.: Radon fluxes from soils to the atmosphere
11 measured by ^{210}Pb - ^{226}Ra disequilibrium in soils, *Geophys Res Lett*, 17, 841-844,
12 1990.

13 Graustein, W.C., and Turekian, K.K.: ^7Be and ^{210}Pb indicate an upper troposphere source for
14 elevated ozone in the summertime subtropical free troposphere of the eastern North
15 Atlantic, *Geophys Res Lett*, 23, 539-542, 1996.

16 Hötzel, H., and Winkler, R.: Activity concentrations of ^{226}Ra , ^{228}Ra , ^{210}Pb , ^{40}K and ^7Be and their
17 temporal variations in surface air, *J Environ Radioactiv*, 5, 445-458, 1987

18 Huang M., Carmichael, G.R., Chai, T., Pierce, R.B., Oltmans, S.J., Jaffe, D.A., Bowman, K.W.,
19 Kaduwela, A., Cai, C., Spak, S.N., Weinheimer, A.J., Huey, L.G., and Diskin, G.S.:
20 Impacts of transported background pollutants on summertime western US air quality:
21 model evaluation, sensitivity analysis and data assimilation, *Atmos Chem Phys*, 13, 359-
22 391, 2013.

23 Ioannidou, A., Manolopoulou, M., and Papastefanou, C.: Temporal changes of ^7Be and ^{210}Pb
24 concentrations in surface air at temperate latitudes (40°), *Appl Radiat Isotopes*, 63(2), 277-
25 284, 2005.

1 Ioannidou, A., Vasileiadis, A., and Melas, D.: Time lag between the tropopause height and ^7Be
2 activity concentrations in surface air, *J Environ Radioactiv*, 129, 80-85, 2014.

3 Jacob, D.J., and Prather, M.J.: Radon-222 as a test of boundary layer convection in a general
4 circulation model, *Tellus B*, 42, 118-134, 1990.

5 James, P., Stohl, A., Forster, C., Eckhardt, S., Seibert, P., and Frank, A., A 15-year climatology
6 of stratosphere-troposphere exchange with a Lagrangian particle dispersion model 2. Mean
7 climate and seasonal variability, *J Geophys Res*, 108(D12), 8522,
8 doi:10.1029/2002JD002639, 2003.

9 Jasiulionis, R., and Wershofen, H.: A study of the vertical diffusion of the cosmogenic
10 radionuclides, ^7Be and ^{22}Na in the atmosphere. *J Environ Radioactiv*, 79, 157-169, 2005.

11 Johnson, W., and Viezee, W., Stratospheric ozone in the lower troposphere: i. Presentation and
12 interpretation of aircraft measurements. *Atmos Environ*, 15, 1309–1323, 1981.

13 Junge, C.E.: Air chemistry and radioactivity. Academic Press, New York, USA, and London,
14 UK, 382 pp, 1963.

15 Kinnison, D.E., Connell, P.S., Rodriguez, J.M., Rotman, D.A., Considine, D.B., Tannahill, J.,
16 Ramarason, R., Rasch, P.J., Douglass, A.R., Baughcum, S.L., Coy, L., Waugh, D.W.,
17 Kawa, S.R., and Prather, M.J.: The Global Modeling Initiative assessment model:
18 Application to high-speed civil transport perturbation, *J Geophys Res*, 106(D2), 1693-
19 1711, 2001.

20 Koch, D.M., Jacob, D.J., and Graustein, W.C.: Vertical transport of tropospheric aerosols as
21 indicated by ^7Be and ^{210}Pb in a chemical tracer model, *J Geophys Res*, 101(D13), 18651-
22 18666, 1996.

23 Koch, D., and Rind, D.: Beryllium10/beryllium7 as a tracer of stratospheric transport, *J*
24 *Geophys Res*, 103, 3907-3917, 1998.

1 Kulan, A., Aldahan, A., Possnert, G., and Vintersved, I.: Distribution of ^7Be in surface air of
2 Europe, *Atmos Environ*, 40, 3855-3868, 2006.

3 Lal, D., Malhotra, P.K., and Peters, B.: On the production of radioisotopes in the atmosphere
4 by cosmic radiation and their application to meteorology, *J Atmos Sol-Terr Phy*, 12, 306-
5 328, 2006.

6 Lal, D., and Peters, B.: Cosmic ray produced radioactivity on the Earth, in: *Handbuch der*
7 *Physik*, 46/2, edited by Sitte, K., Springer-Verlag, New York, USA, pp. 551-561, 1967.

8 Lee, H. N., Wan, G., Zheng, X., Sanderson, C.G., Josse, B., Wang, S., Yang, W., Tang, J., and
9 Wang, C.: Measurements of ^{210}Pb and ^7Be in China and their analysis accompanied with
10 global model calculations of ^{210}Pb , *J Geophys Res*, 109, D22203,
11 doi:10.1029/2004JD005061, 2004.

12 Lee, H. N., Tositti, L., Zheng, X., and Bonasoni, P.: Analyses and comparisons of variations
13 of ^7Be , ^{210}Pb and $^7\text{Be}/^{210}\text{Pb}$ with ozone observations at two Global Atmosphere Watch
14 stations from high mountains, *J Geophys Res*, 112, D05303, doi:10.1029/2006JD007421,
15 2007

16 Lelieveld, J., Berresheim, H., Borrmann, S., Crutzen, P.J., Dentener, F.J., Fischer, H., Feichter,
17 J., Flatau, P.J., Heland, J., Holzinger, R., Kormann, R., Lawrence, M.G., Levin, Z.,
18 Markowicz, K.M., Mihapoulos, N., Minikin, A., Ramanathan, V., de Reus, M., Roelofs,
19 G.J., Scheeren, H.A., Sciare, J., Schlager, H., Schultz, M., Siegmund, P., Steil, B.,
20 Stephanou, E.G., Stier, P., Traub, M., Warneke, C., Williams, J., and Ziereis, H.: Global
21 air pollution crossroads over the Mediterranean. *Science*, 298, 794-799, 2002.

22 Li, Q., Jacob, D.J., Logan, J.A., Bey, I., Yantosca, R.M., Liu, H., Martin, R.V., Fiore, A.M.,
23 Field, B.D., Duncan, B.N.: A Tropospheric Ozone Maximum Over the Middle East,
24 *Geophys Res Lett*, 28(17), 3235-3238, 2001.

1 Likuku, A.S.: Factors influencing ambient concentrations of ^{210}Pb and ^7Be over the city of
2 Edinburgh (55.9°N, 03.2°W), *J Environ Radioactiv*, 87, 289-304, 2006.

3 Liu, H., Jacob, D.J., Bey, I., and Yantosca, R.M.: Constraints from the ^{210}Pb and ^7Be on wet
4 deposition and transport in a global three-dimensional chemical tracer model driven by
5 assimilated meteorological fields, *J Geophys Res*, 106, D11, 12109-12128, 2001.

6 Liu, H., Jacob, D.J., Dibb, J.E., Fiore, A.M., and Yantosca, R.M.: Constraints on the sources
7 of tropospheric ozone from ^{210}Pb - ^7Be - O_3 correlations, *J Geophys Res*, 109(D07306),
8 doi:10.1029/2003JD003988, 2004.

9 Liu, H., Considine, D. B., Horowitz, L. W., Crawford, J. H., Rodriguez, J. M., Strahan, S. E.,
10 Damon, M. R., Steenrod, S. D., Xu, X., Kouatchou, J., Carouge, C., and Yantosca, R. M.:
11 Using beryllium-7 to assess cross-tropopause transport in global models, *Atmos. Chem.*
12 *Phys.*, 16, 4641-4659, doi:10.5194/acp-16-4641-2016, 2016.

13 Lozano, R.L., Hernández-Ceballos, M.A., San Miguel, E.G., Adame, J.A., and Bolívar, J.P.:
14 Meteorological factors influencing the ^7Be and ^{210}Pb concentrations in surface air from the
15 southwestern Iberian Peninsula, *Atmos Environ*, 63, 168-178, 2012.

16 Lozano, R.L., Hernández-Ceballos, M.A., Rodrigo, J.F., San Miguel, E.G., Casas-Ruiz, M.,
17 García-Tenorio, R., and Bolívar, J.P.: Mesoscale behavior of ^7Be and ^{210}Pb in superficial
18 air along the Gulf of Cadiz (south of Iberian peninsula), *Atmos Environ*, 80, 75-84, 2013.

19 Marinoni, A., Cristofanelli, P., Calzolari, F., Roccato, F., Bonafé, U., and Bonasoni, P.:
20 Continuous measurements of aerosol physical parameters at the Mt. Cimone GAW Station
21 (2165 m asl, Italy), *Sci Total Environ*, 391, 241-251, 2008.

22 Millán, M., Sanz, J., Salvador, R., and Mantilla, E.: Atmospheric dynamics and ozone cycles
23 related to nitrogen deposition in the western Mediterranean, *Environ Pollut*, 118, 167-186,
24 2006.

1 Monks, P.S., Granier, C., Fuzzi, S., Stohl, A., Williams, M.L., Akimoto, H., Amann, M.,
2 Baklanov, A., Baltensperger, U., Bey, I., Blake, N., Blake, R.S., Carslaw, K., Cooper, O.R.,
3 Dentener, F., Fowler, D., Fragkou, E., Frost, G.J., Generoso, S., Ginoux, P., Grewe, V.,
4 Guenther, A., Hansson, H.C., Henne, S., Hjorth, J., Hofzumahaus, A., Huntrieser, H.,
5 Isaksen, I.S.A., Jenkin, M.E., Kaiser, J., Kanakidou, M., Klimont, Z., Kulmala, M., Laj, P.,
6 Lawrence, M.G., Lee, J.D., and Liousse, C.: Atmospheric composition change – global and
7 regional air quality, *Atmos Environ*, 43, 5268-5350, 2009.

8 Moore, H.E., Poet, S.E., and Martell, E.A.: ^{222}Rn , ^{210}Pb , ^{210}Bi , and ^{210}Po , profiles and aerosol
9 residence times versus altitude, *J Geophys Res*, 78, 7065-7075, 1973.

10 Nazaroff, W.W.: Radon transport from soil to air, *Rev Geophys*, 30, 137-160, 1992.

11 ORTEC: Gamma-Vision 32 A66-B32 user's manual. ORTEC USA, Part No. 783620, Manual
12 Revision D, 2003.

13 Papastefanou, C., and Ioannidou, A.: Aerodynamic size association of ^7Be in ambient aerosols.
14 *J Environ Radioactiv*, 26, 273-282, 1995.

15 Pham, M.K., Betti, M., Nies, H., and Povinec, P.P.: Temporal changes of ^7Be , ^{137}Cs and ^{210}Pb
16 activity concentrations in surface air at Monaco and their correlation with meteorological
17 parameters, *J Environ Radioactiv*, 102, 1045-1054, 2011.

18 Rastogi, N., and Sarin, M.M.: Atmospheric ^{210}Pb and ^7Be in ambient aerosols over low- and
19 high-altitude sites in 34 semiarid region: Temporal variability and transport processes, *J*
20 *Geophys Res*, 113, doi:10.1029/2007JD009298, 2008.

21 Rehfeld, S., and Heimann, M.: Three dimensional atmospheric transport simulation of the
22 radioactive tracers ^{210}Pb , ^7Be , ^{10}Be , and ^{90}Sr , *J Geophys Res*, 100 (D12), 26141-26161,
23 1995.

24 Reiter, E.R.: Weather phenomena of the Mediterranean basin. Part 1. General description of
25 the meteorological processes, In: *Handbook for forecasters in the Mediterranean basin*,

1 Environment Prediction Research Facility, Naval Postgraduate School, Monterey,
2 California, U.S. Department of Commerce, available at [http://www.dtic.mil/cgi-](http://www.dtic.mil/cgi-bin/GetTRDoc?AD=ADA024271)
3 [bin/GetTRDoc?AD=ADA024271](http://www.dtic.mil/cgi-bin/GetTRDoc?AD=ADA024271), last accessed 15 March 2016, 1975.

4 Reiter, R., Sladkovich, K., Pötzl, K., Carnuth, W., and Kanter H.J.: Studies on the influx of
5 stratospheric air into the lower troposphere using cosmic-ray produced radionuclides and
6 fallout, *Arch Meteor Geophy A*, Vol.20(3), 211-246, 1971.

7 Reiter, R., Munzert, K., Kanter, H.-J., and Pötzl, K.: Cosmogenic radionuclides and ozone at a
8 mountain station at 3.0 km a.s.l., *Arch Meteor Geophy B*, 32, 131-160, 1983.

9 Rienecker, M.M., Suarez, M.J., Gelaro, R., Todling, R., Bacmeister, J., Liu, E., Bosilovich,
10 M.G., Schubert, S.D., Takacs, L., Kim, G.-K., Bloom, S., Chen, J., Collins, D., Conaty, A.,
11 da Silva, A., Gu, W., Joiner, J., Koster, R.D., Lucchesi, R., Molod, A., Owens, T., Pawson,
12 S., Pegion, P., Redder, C.R., Reichle, R., Robertson, F.R., Ruddick, A.G., Sienkewicz, M.,
13 and Woollen, J.: MERRA: NASA's Modern-Era Retrospective Analysis for Research and
14 Applications. *J Climate*, 24(14), 3624-3648, 2011.

15 Rodriguez, J.M., Logan, J.A., Bergmann, D., Megretskaja, I., Jacob, D.J., Xie, H., Das, B., and
16 Strahan, S.E.: The impact of meteorological fields on tropospheric ozone distributions
17 calculated by the Global Modeling Initiative (GMI) chemical-transport model, in:
18 Quadrennial Ozone Symposium QOS 2004, edited by: Zerefos, C., pp.147, International
19 Ozone Commission, Kos, Greece, 2004

20 Rotman, D.A., Tannahill, J.R., Kinnison, D.E., Connell, P.S., Bergmann, D., Proctor, D.,
21 Rodriguez, J.M., Lin, S.J., Rood, R.B., Prather, M.J., Rasch, P.J., Considine, D.B.,
22 Ramarason, R., and Kawa, S.R.: Global Modeling Initiative assessment model: Model
23 description, integration, and testing of the transport shell, *J Geophys Res*, 106(D2), 1669-
24 1691, 2001.

1 Schery, S.D., Whittlestone, S., Hart, K.P., and Hill, S.E.: The flux of radon and thoron from
2 Australian soils, *J Geophys Res*, 100, 26141-26161, 1989.

3 SILSO (Sunspot Index and Long-term Solar Observation), World Data Center – Sunspot
4 Number and Long-Term Solar Observations, Royal Observatory of Belgium, on-line
5 Sunspot Number catalogue, available at <http://sidc.oma.be/silso/>, last accessed 15 March
6 2016

7 Simon, J., Meresova, J., Sykora, I., Jeskovsky, M., and Holy, K.: Modeling of temporal
8 variations of vertical concentration profile of ^7Be in the atmosphere. *Atmos Environ*, 43,
9 2000-2004, 2009.

10 Steinmann, P., Zeller, M., Beuret, P., Ferreri, G., and Estier, S.: Cosmogenic ^7Be and ^{22}Na in
11 ground level air in Switzerland (1994-2011), *J Environ Radioactiv*, 124, 68-73, 2013.

12 Stohl, A., Wernli, H., James, P., Borqui, M., Forster, C., Liniger, M.A., Seibert, P., and
13 Sprenger, M.: A new perspective of stratosphere-troposphere exchange, *Bull Am Meteor*
14 *Soc*, 84, 1565-1573 DOI: 10.1175/BAMS-84-11-1565, 2003.

15 Strahan, S.E., Duncan, B.N., and Hoor, P.: Observationally-derived diagnostics of transport in
16 the lowermost stratosphere and their application to the GMI chemistry transport model.
17 *Atmos Chem Phys*, 7, 1435-2445, 2007

18 Todorovic, D., Popovic, D., Djuric, G., Radenkovic, M.: ^7Be to ^{210}Pb concentration ratio in
19 ground level air in Belgrade area, *J Environ Radioactiv*, 79, 297-307, 2005.

20 Tositti, L., Riccio, A., Sandrini, S., Brattich, E., Baldacci, D., Parmeggiani, S., Cristofanelli,
21 P., and Bonasoni, P.: Short-term climatology of PM10 at a high altitude background station
22 in southern Europe, *Atmos Environ*, 65, 145-152, 2013.

23 Tositti, L., Brattich, E., Cinelli, G., and Baldacci, D.: 12 years of ^7Be and ^{210}Pb data in Mt.
24 Cimone, and their correlation with meteorological parameters, *Atmos Environ*, 87C, 108-
25 122. doi: 10.1016/j.atmosenv.2014.01.014, 2014.

1 Trickl, T., Feldmann, H., Kanter, H.-J., Scheel, H.-E., Sprenger, M., Stohl, A. and Wernli, H.,
 2 2010. Forecasted deep stratospheric intrusions over central Europe: case studies and
 3 climatologies, *Atmos Chem Phys*, 10, 499-524.
 4 Trigo, I.F., Bigg, G.R., and Davies, T.D.: Climatology of cyclogenesis mechanisms in the
 5 Mediterranean. *Mon Weather Rev*, 130, 549-569, 2002.
 6 Turekian, K.K., Nozaki, Y., and Benninger, L.K.: Geochemistry of atmospheric radon and
 7 radon products. *Annu Rev Earth Pl Sc*, 5, 227-255, 1977.
 8 Turekian, K.K., and Graustein, W.C.: Natural Radionuclides in the Atmosphere, in: *Treatise*
 9 *on Geochemistry*, Volume 4, Ralph Keeling, F. (Ed.), Holland, H.D., and Turekian, K.K.
 10 (executive editors), pp. 347, doi:10.1016/B0-08-043751-6/04042-1, ISBN 0-08-043751-6.
 11 Elsevier, p.261-279, 2003.
 12 Usoskin, I., and Kovaltsov, G.: Production of cosmogenic ^7Be isotope in the atmosphere: full
 13 3D modelling. *J Geophys Res*, 113, D12107, 2008.
 14 van Dingenen, R., Putaud, J.P., Martins-Dos Santos, S., Raes, F. Physical aerosol properties
 15 and their relation to air mass origin at Monte Cimone (Italy) during the first MINATROC
 16 campaign, *Atmos Chem Phys*, 5, 2203-2226, 2005.
 17 Viezee, W., and Singh, H.B.: The distribution of beryllium-7 in the troposphere. Implications
 18 on stratosphere/tropospheric air exchange, *Geophys Res Lett*, 7, 805-808, 1980.
 19 Wilkening, M.H., Clements, W.E., and Stanley, D.: Radon-222 flux measurements in widely
 20 separated regions, In: *The Natural Radiation Environment II*, pp. 717-730, U.S. Energy and
 21 Res. Dev. Admin., Oak Ridge, Tenn, USA, 1975.
 22 Winkler, R., Dietl, F., Frank, G., and Thiersch, J.: Temporal variation of ^7Be and ^{210}Pb size
 23 distributions in ambient aerosols, *Atmos Environ*, 32, 983-991, 1998.
 24 WMO-GAW (World Meteorological Organization - Global Atmosphere Watch): 1st
 25 International Expert Meeting on Sources and Measurements of Natural Radionuclides

Applied to Climate and Air Quality Studies, (Gif-sur-Yvette, France, 3-5 June 2003) (WMO
TD No. 1201), Report No. 155 [available at
<ftp://ftp.wmo.int/Documents/PublicWeb/arep/gaw/gaw155.pdf>, last accessed 15 March
2016], 2004

Zanis, P., Schuepbach, E., Gäggeler, H.W., Huebener, S., and Tobler, L.: Factors controlling
Beryllium-7 at Jungfraujoch in Switzerland, *Tellus*, 51 (4), 789-805, 1999.

Zanis, P., Monks, P.S., Schuepbach, R., Carpenter, L.J., Green, T.J., Mills, G.P., Bauguitte, S.,
and Penkett, S.A.: In situ ozone production under free tropospheric conditions during
FREETEX '98 in the Swiss Alps, *J Geophys Res*, 105 (D1), 24223-24234, 2000.

Zanis, P., Gerasopoulos, E., Priller, A., Schnabel, C., Stohl, A., Zerefos, C., Gäggeler, H.W.,
Tobler, L., Kubik, P.W., Kanter, H.J., Scheel, H.E., Luterbacher, J., and Berger, M.: An
estimate of the impact of stratosphere-to-troposphere transport (STT) on the lower free
tropospheric ozone over the Alps using ^{10}Be and ^7Be measurements, *J Geophys Res*,
108(D12), 8520, doi:10.1029/2002JD002604, 2003.

1
2
3
4
5
6
7
8
9
10
11
12
13
14

Figures

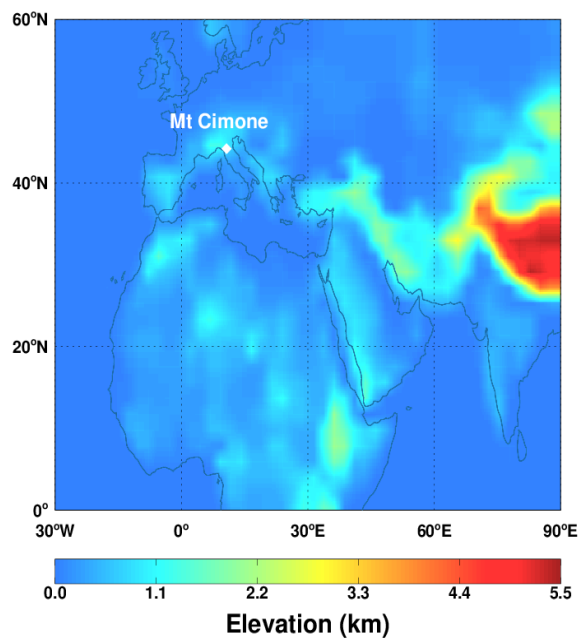
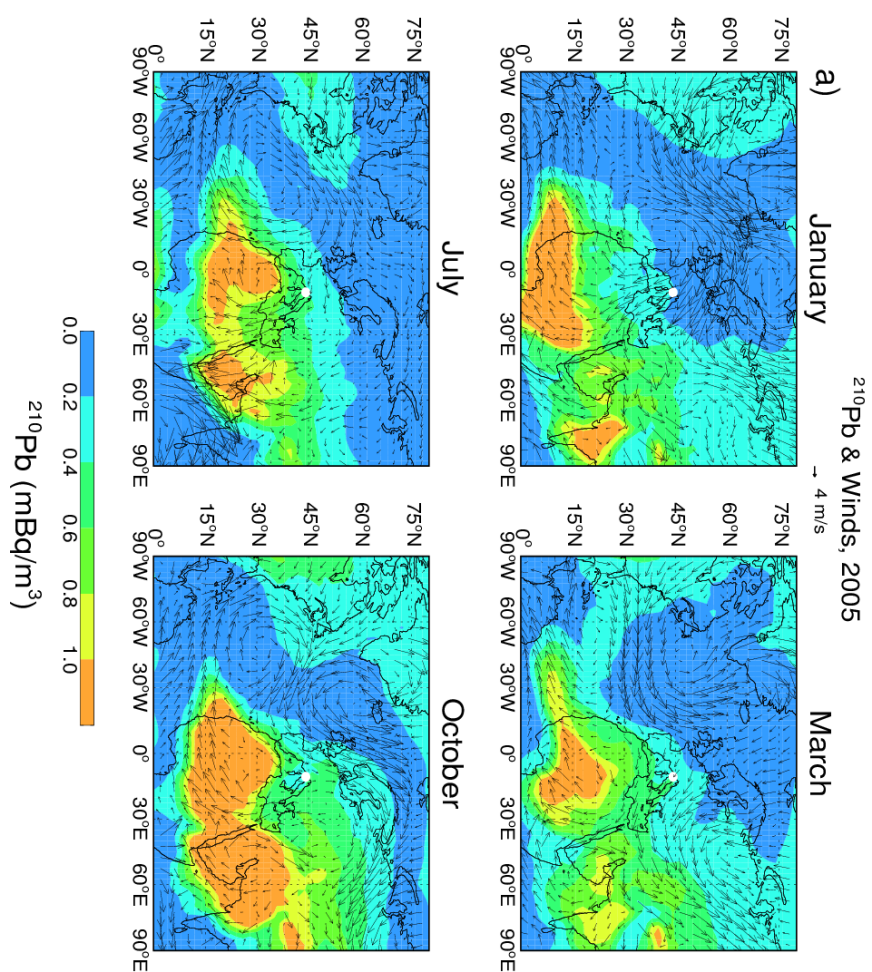


Figure 1. Surface elevations (km) in the model. The white dot indicates the location of Mt. Cimone (44°12' N, 10°42' E, 2165 m asl).



1

2 **Figure 2.** Simulated monthly mean (a) ^{210}Pb concentrations and (b) ^7Be concentrations, at the

3 elevation of Mt. Cimone. Arrows represent the seasonality of winds in the MERRA

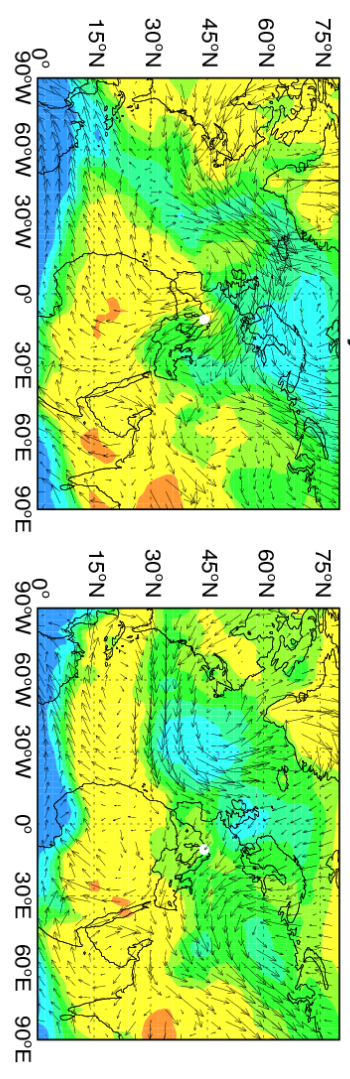
4 meteorological data. The white dot indicates the location of Mt. Cimone (44°12' N, 10°42' E,

5 2165 m asl). To be continued.

b)

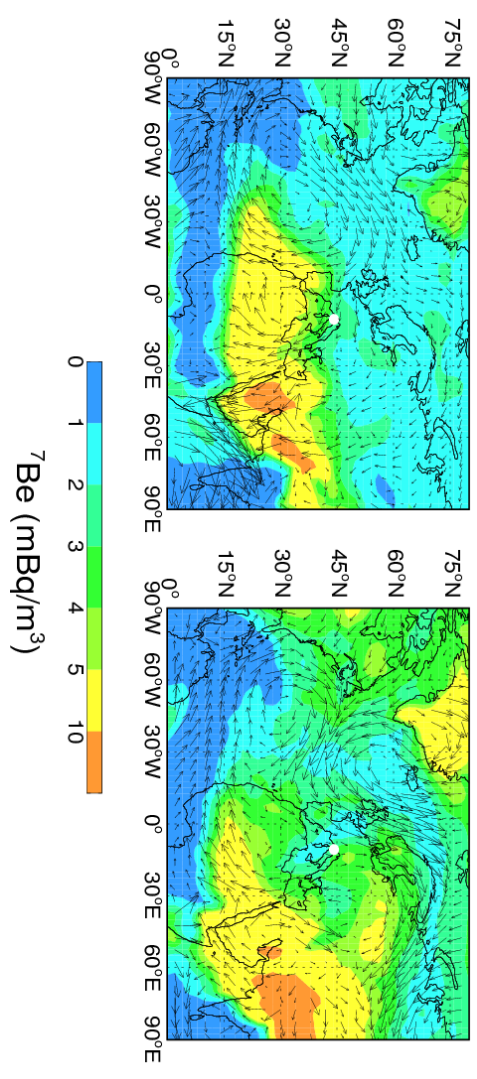
January

March

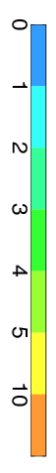


July

October



⁷Be (mBq/m³)



1
2
3

Figure 2. (continued)

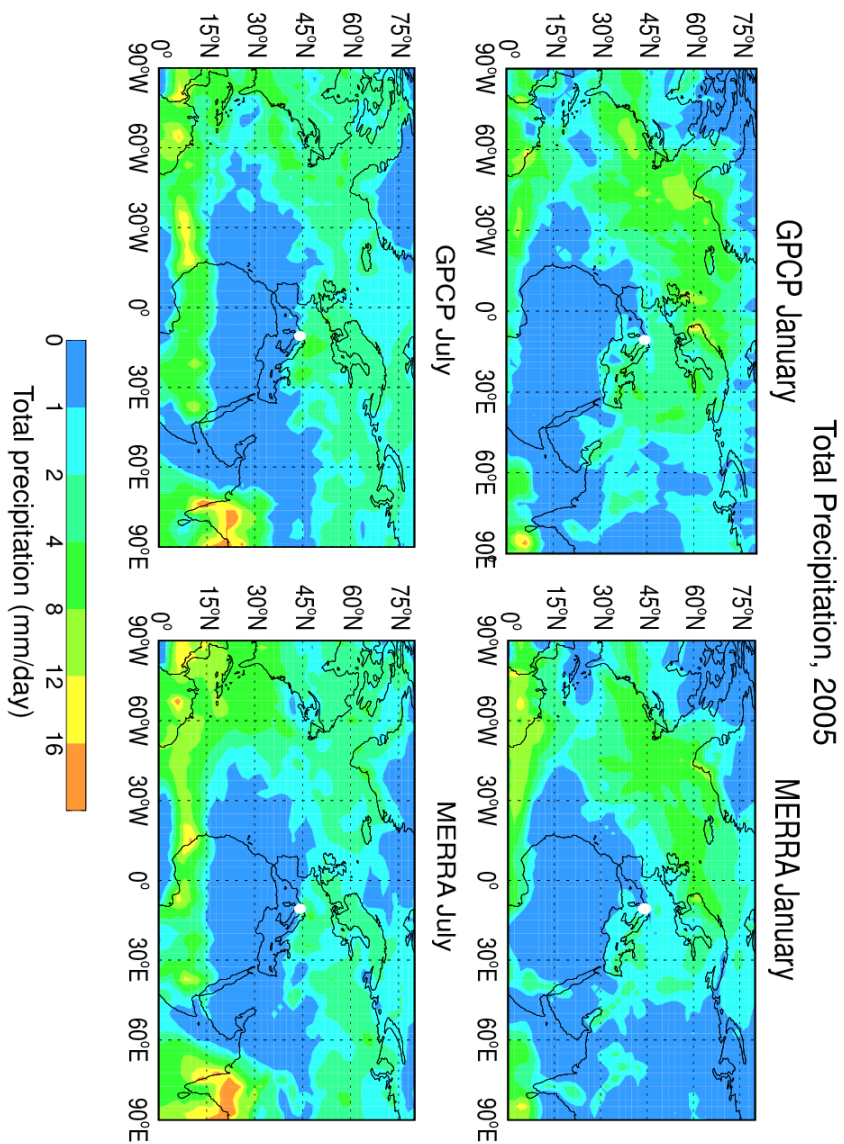


Figure 3. Comparison of the MERRA total precipitation (0-75°N, 90°W-90°E) during January and July 2005 with that in the GPCP observations. The white dot indicates the location of Mt. Cimone (44°12'N, 10°42'E, 2165 m asl).

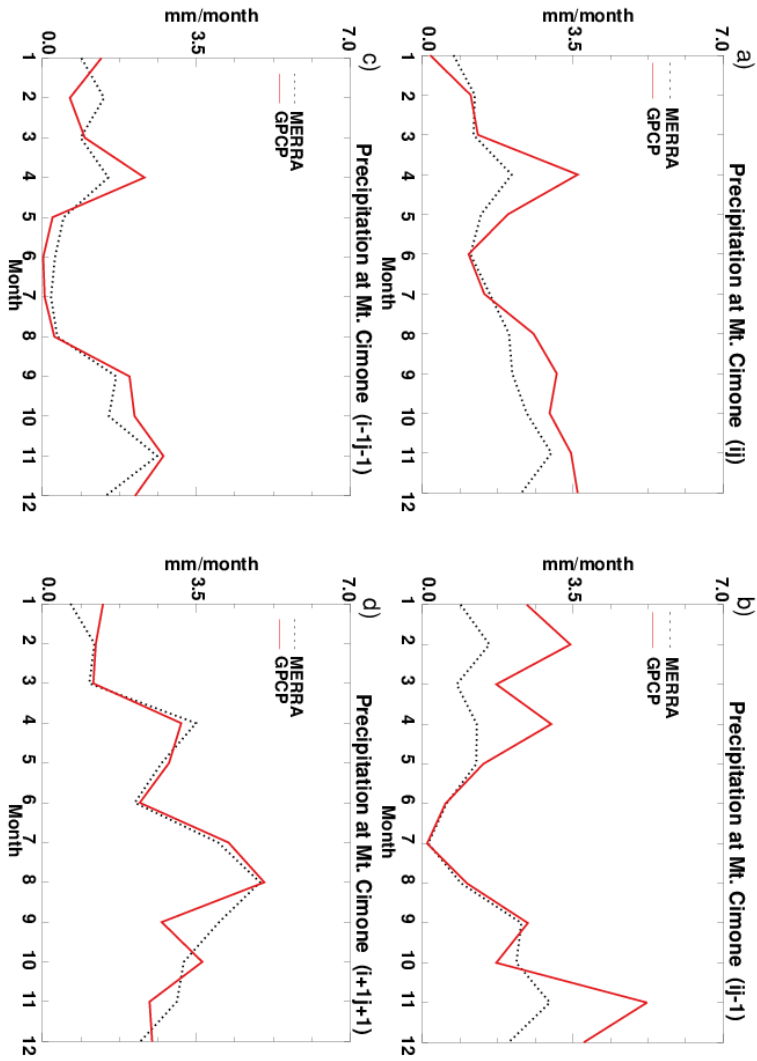
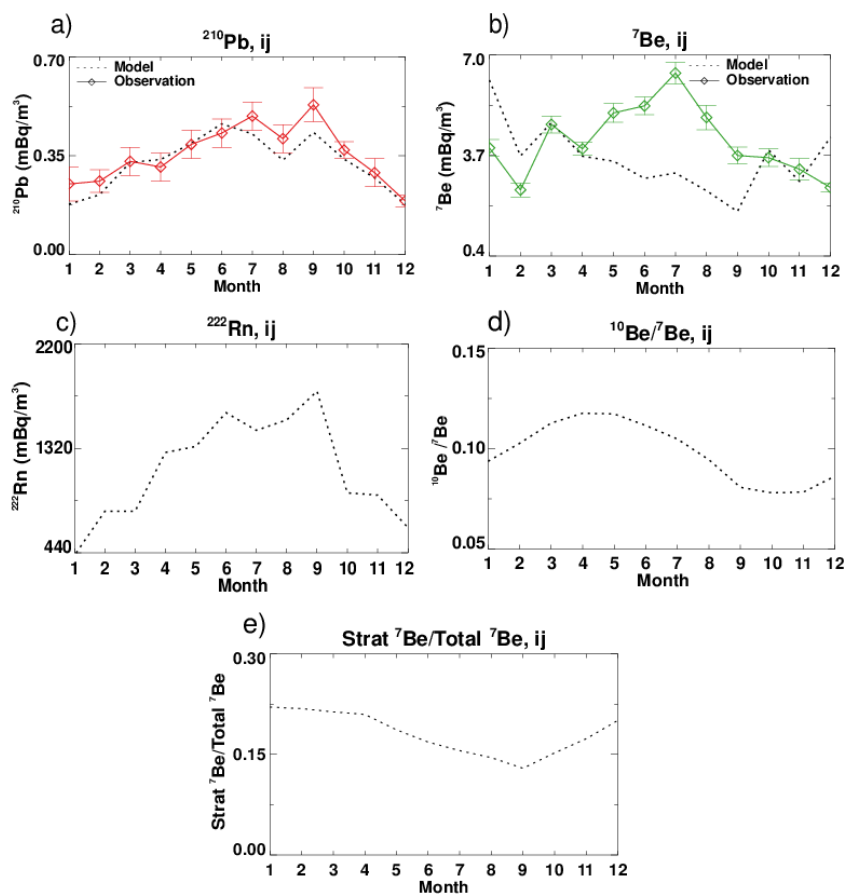


Figure 4. Comparison of the seasonal precipitation at Mt. Cimone in the MERRA meteorological data set with that in the GPCP observations for (a) the model gridbox (“ij”) corresponding to the location of Mt. Cimone, (b) the model gridbox (“ij-1”) to the west of “ij”, (c) the model gridbox (“i-1j-1”) to the southwest of “ij”, and (d) the model gridbox (“i+1j+1”) to the northeast of “ij”.



1
2 **Figure 5 (a,b,c,d,e).** Comparison of GMI simulated (black dotted line) monthly (a) ^{210}Pb and
3 (b) ^7Be activities with those observed at Mt. Cimone (solid lines) in 2005. Also shown are GMI
4 simulated monthly activities of (c) ^{222}Rn , (d) $^{10}\text{Be}/^7\text{Be}$ ratios, and (e) strat $^7\text{Be}/\text{total } ^7\text{Be}$ ratios.
5 Model values are for the “ij” gridbox corresponding to the location of Mt. Cimone. Vertical
6 bars indicate the uncertainty in observed activities.

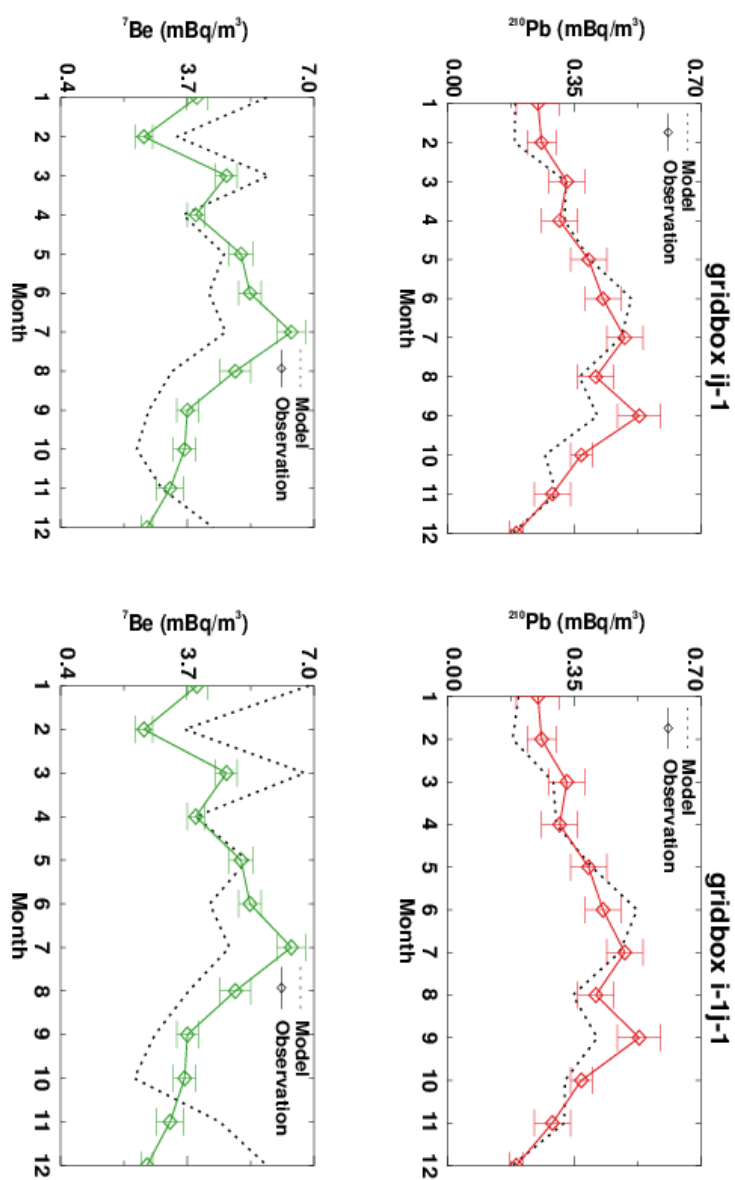


Figure 6. Same as Figure 5(ab), but for the “ij-1” to the south of “ij” (left column) and “i-1j-1” to the southwest of “ij” (right column) grids, respectively.

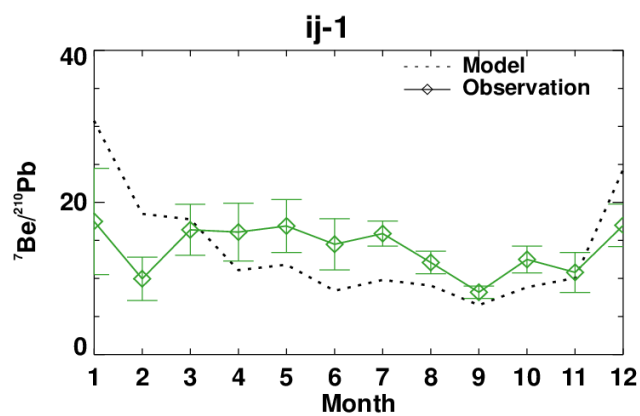
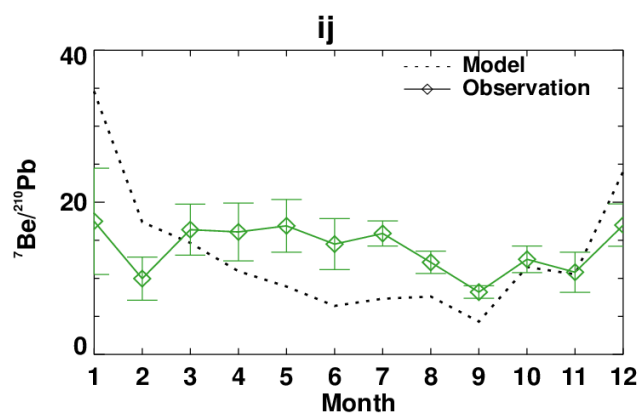
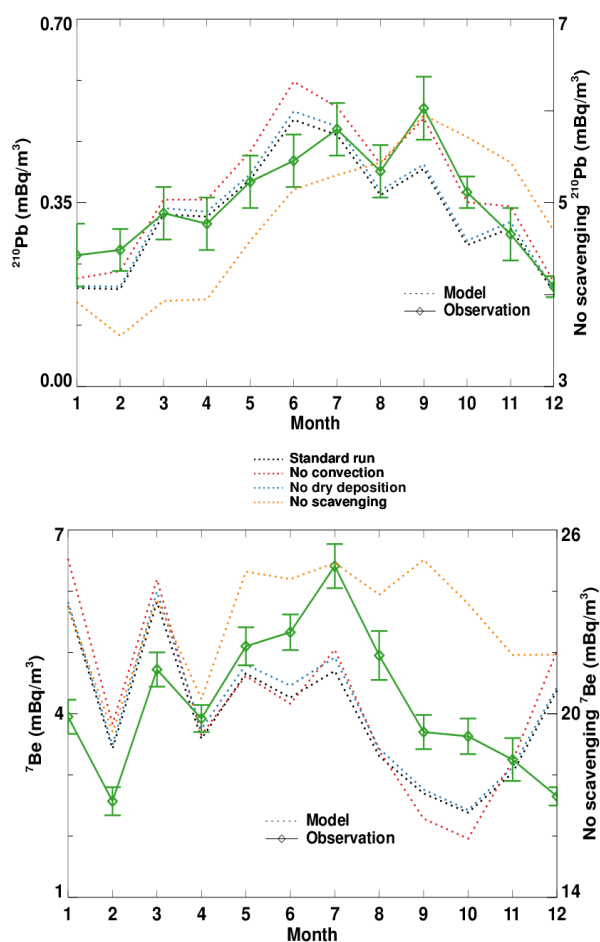


Figure 7. Comparison between GMI simulated monthly ${}^7\text{Be}/{}^{210}\text{Pb}$ ratios at the “ij” and “ij-1” grids (black dotted line) and those from the observations at Mt. Cimone (green solid line). Vertical bars indicate the uncertainty in observed activities.



1

2 **Figure 8.** Comparison of GMI simulated monthly ^{210}Pb and ^7Be activities at Mt. Cimone

3 between the standard (black dotted line) and the sensitivity runs (“ij-1” grid). The sensitivity

4 runs are those without convective transport/scavenging (red dotted line), without dry deposition

5 (blue dotted line), and without scavenging (orange dotted line; y-axis on the right). The

6 observations are shown as green solid line. Vertical bars indicate the uncertainty in observed

7 activities.

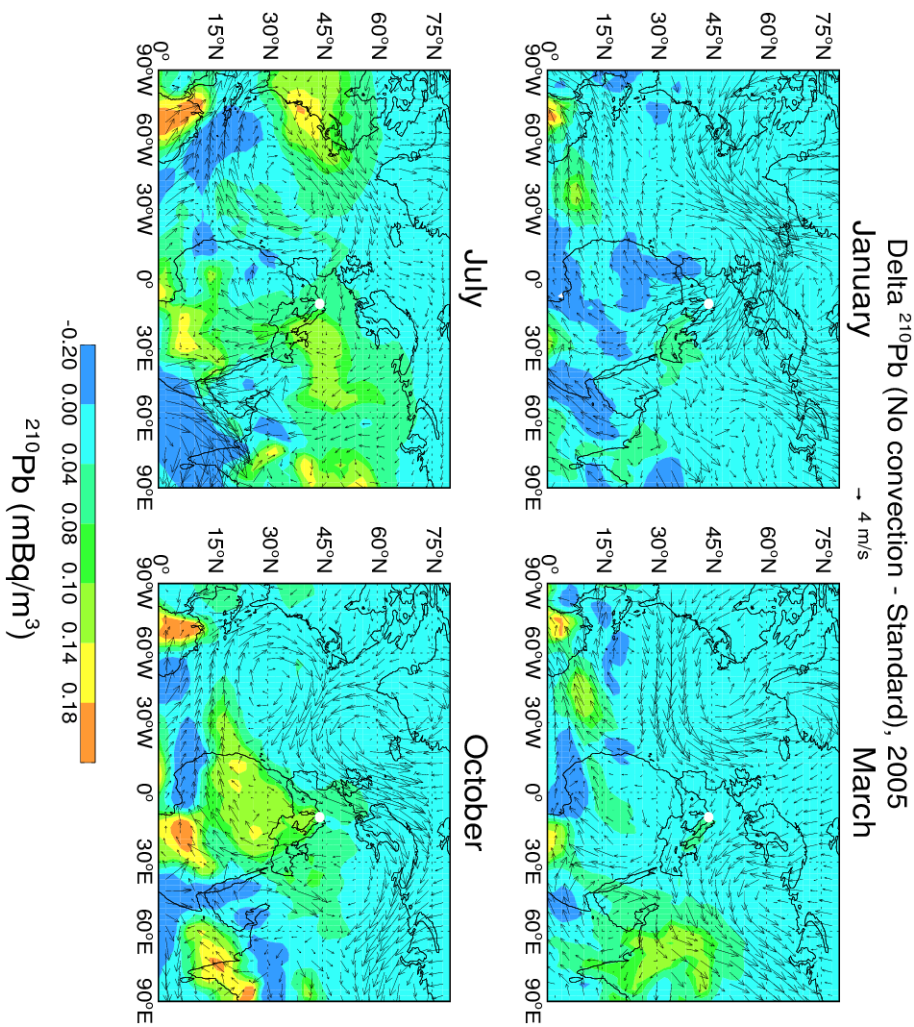


Figure 9. GMI simulated differences of ^{210}Pb concentrations at the elevation of Mt. Cimone between a sensitivity run without convection (i.e., without transport and scavenging in convective updrafts) and the standard run. Arrows denote MERRA winds. The white dot indicates the location of Mt. Cimone (44°12' N, 10°42' E, 2165 m asl).

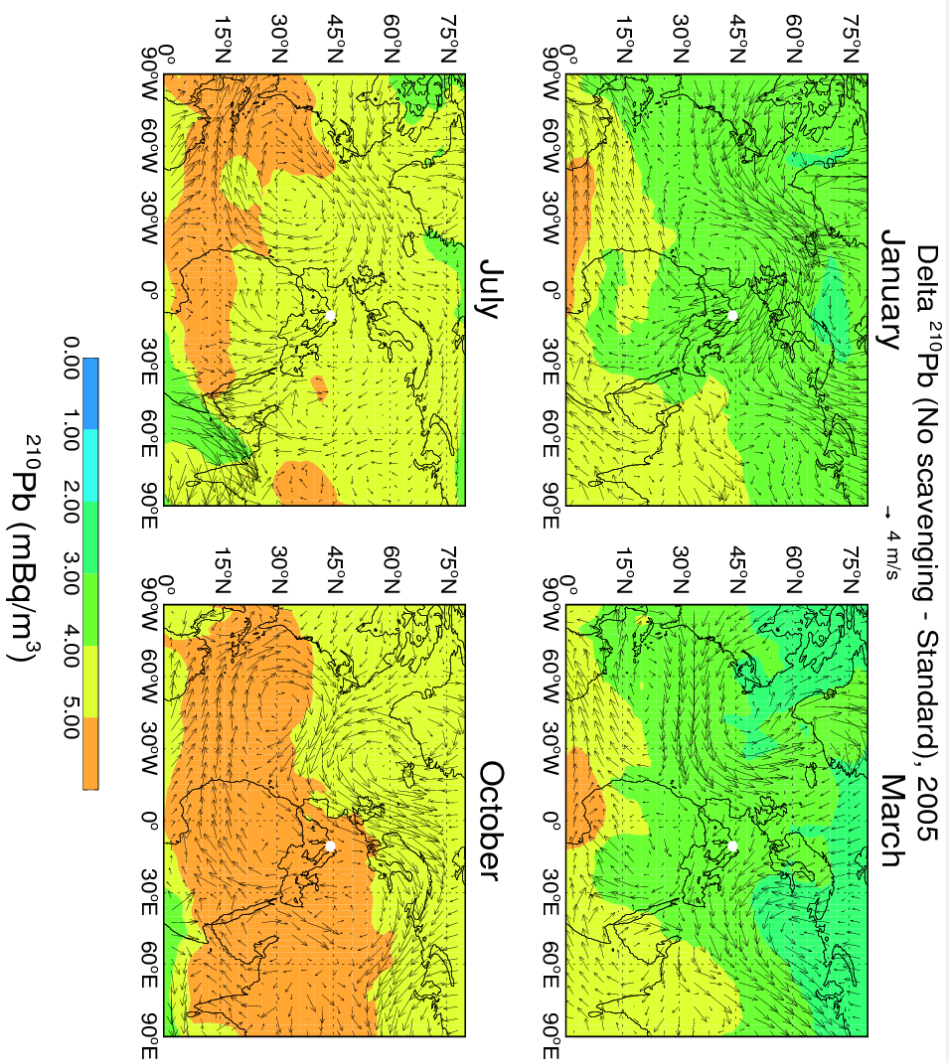
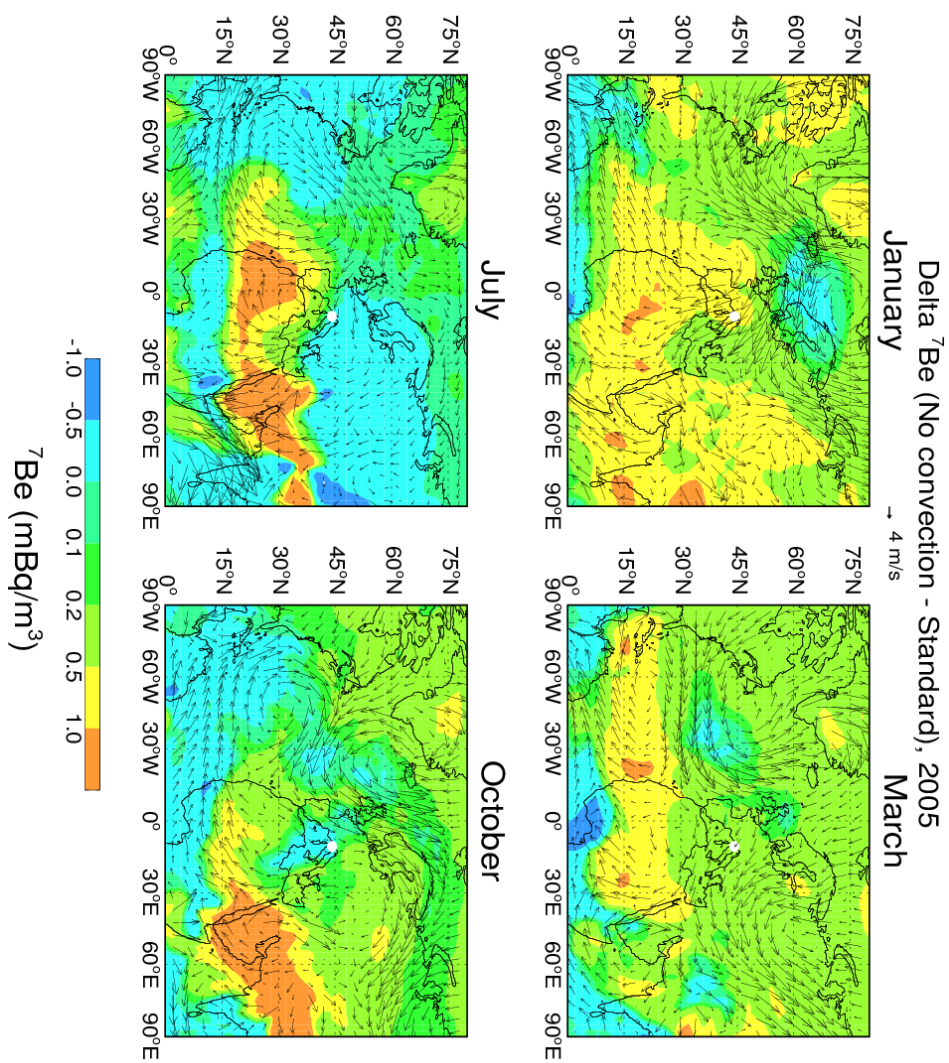


Figure 10. Same as Figure 9, but for a sensitivity simulation where wet scavenging is turned off.



1 **Figure 11.** GMI simulated differences of ^7Be concentrations at the elevation of Mt. Cimone
2 between a sensitivity run without convection and the standard run. Arrows denote MERRA
3 winds. The white dot indicates the location of Mt. Cimone (44°12' N, 10°42' E, 2165 m asl).

4

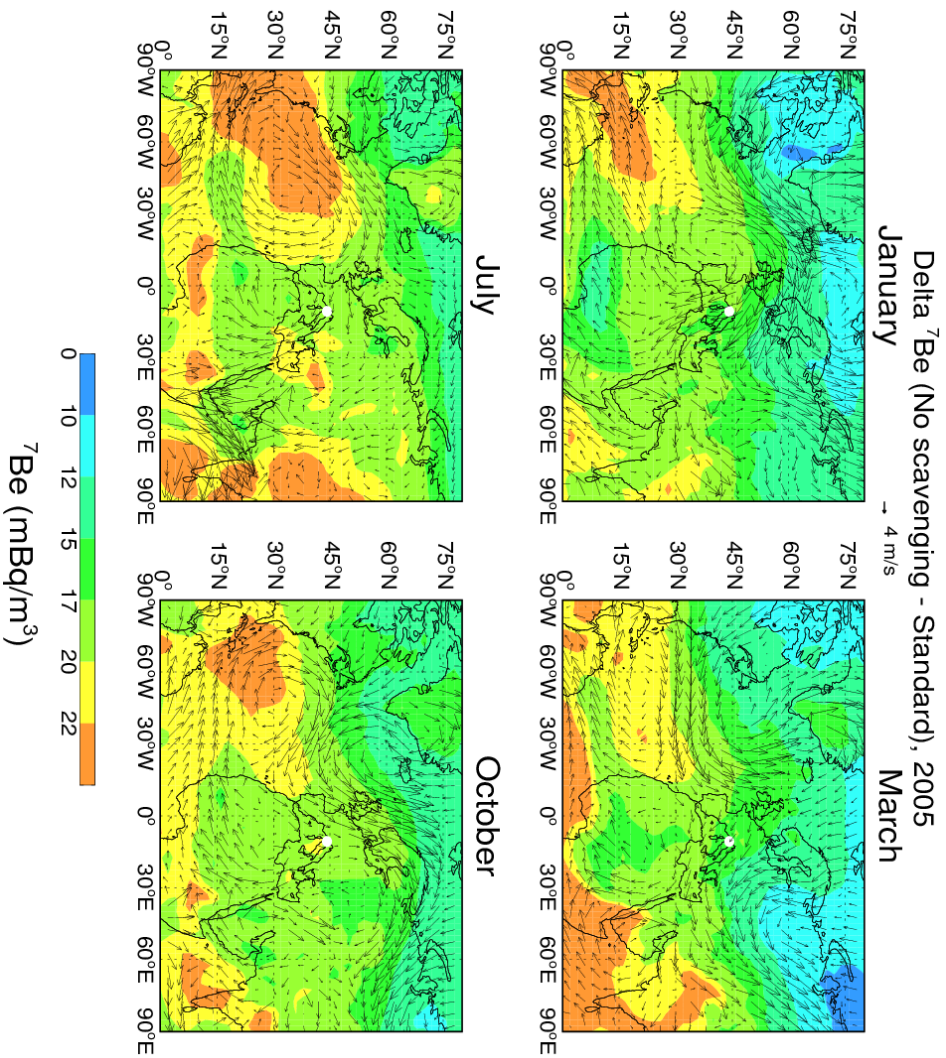
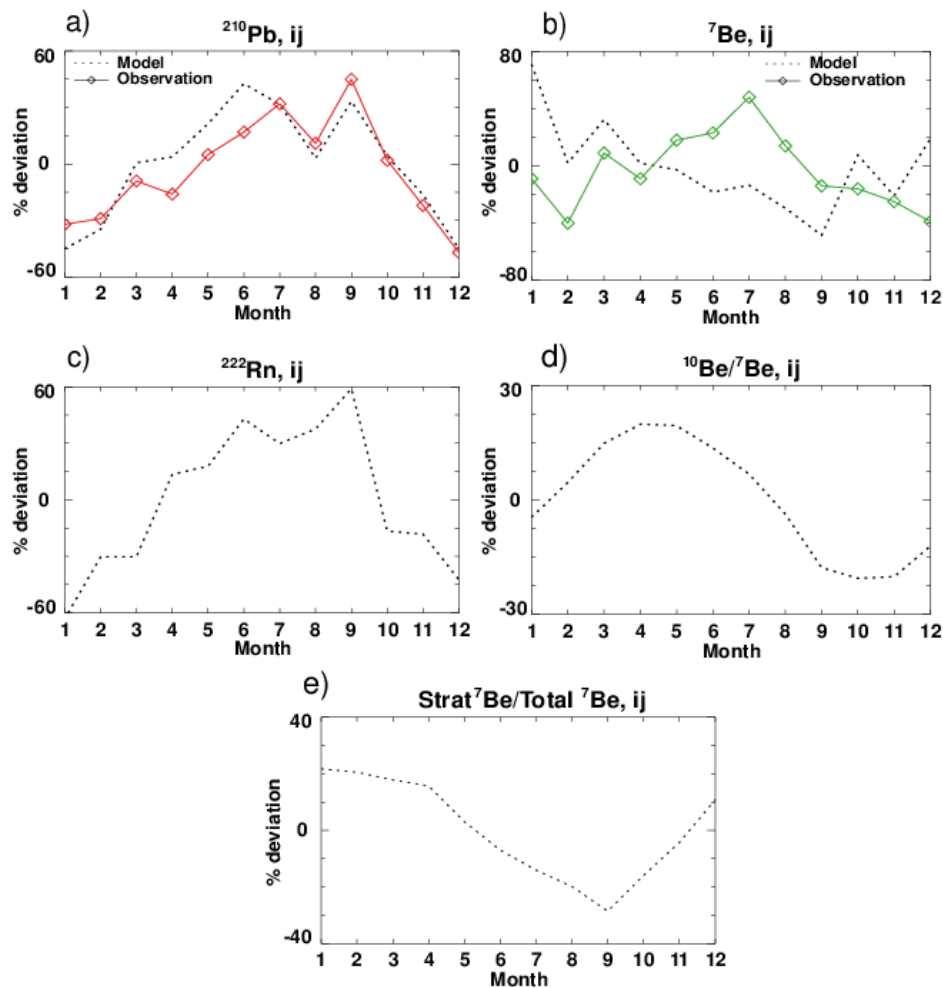
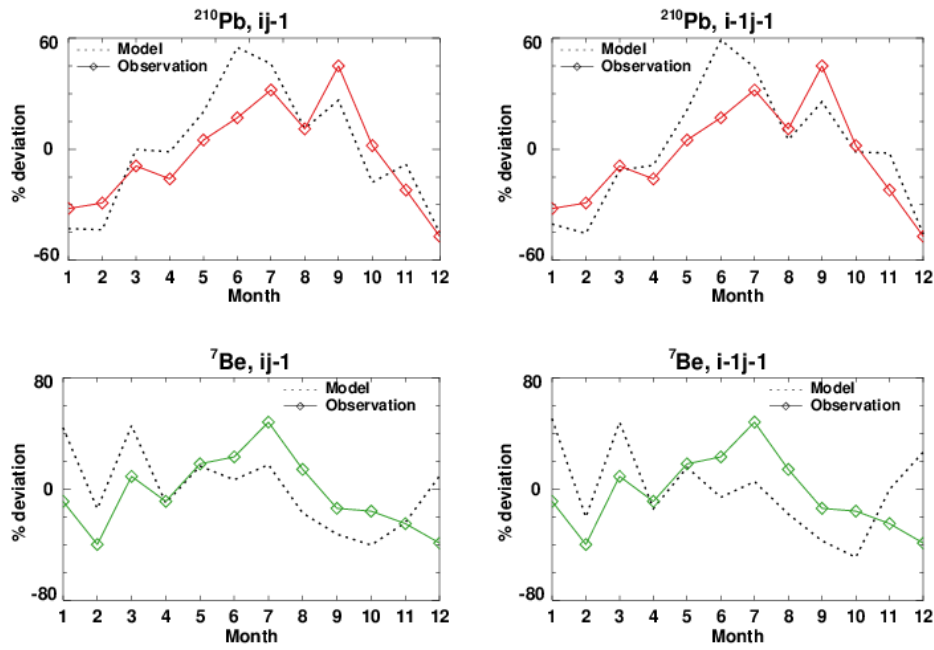


Figure 12. Same as Figure 11 but for the difference between a sensitivity run without wet scavenging and the standard run.

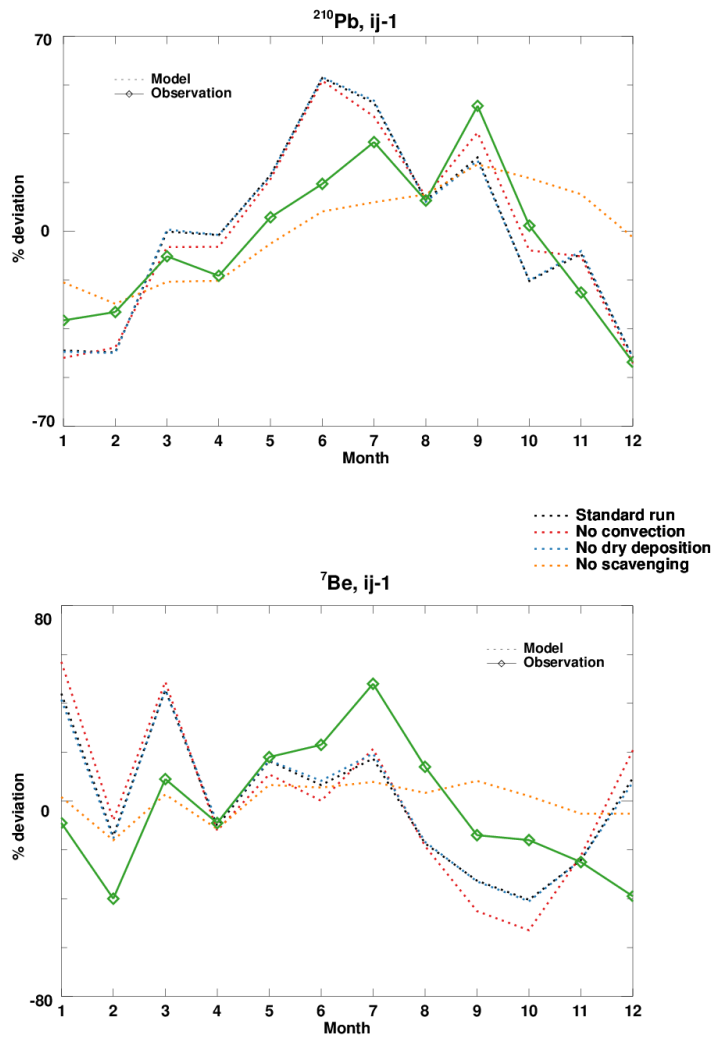
1 Supplementary Material



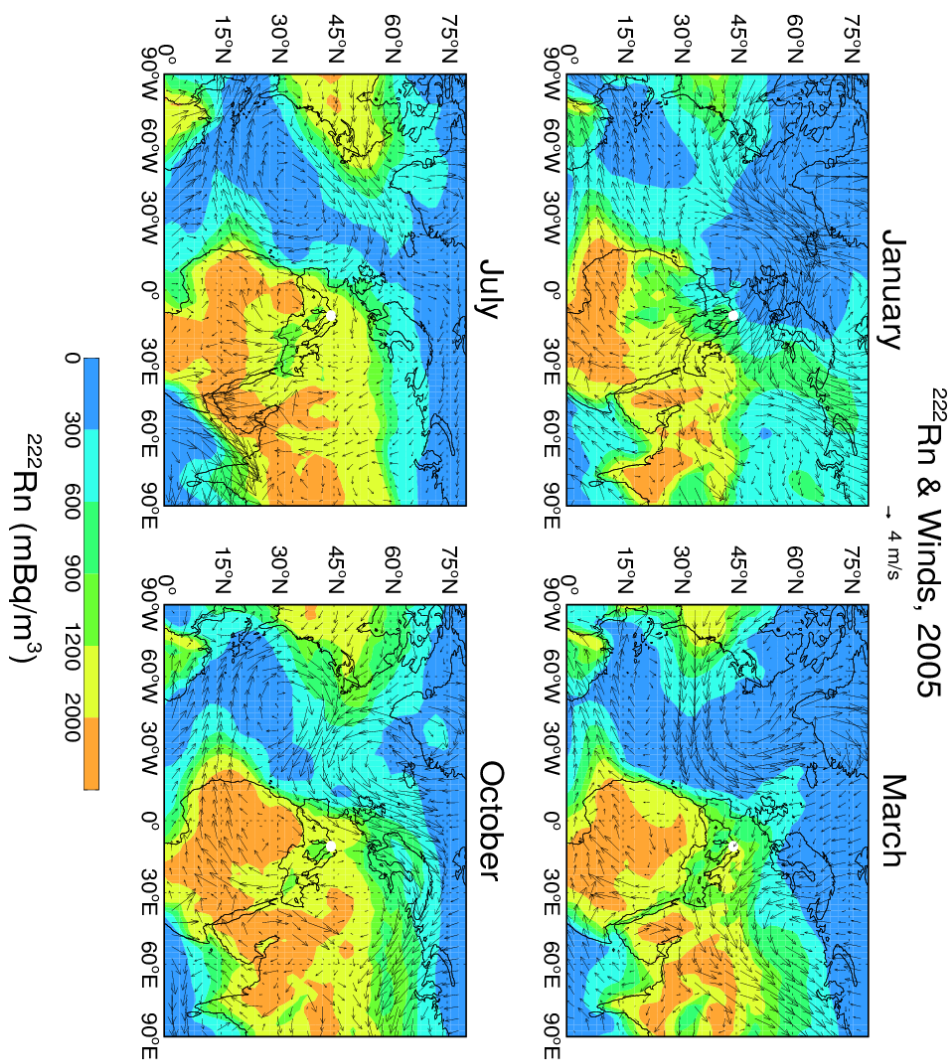
2
3 **SI Figure 1 (a,b,c,d,e).** Comparison of GMI simulated (black dotted line) percentage
4 deviations from the annual means of (a) ^{210}Pb and (b) ^7Be concentrations with those observed
5 at Mt. Cimone (solid lines). Model values are for the “ij” gridbox corresponding to the location
6 of Mt. Cimone. Also shown are GMI simulated monthly fluctuations of (c) ^{222}Rn activities, (d)
7 $^{10}\text{Be}/^7\text{Be}$ ratios and (e) strat ^7Be /total ^7Be ratios.



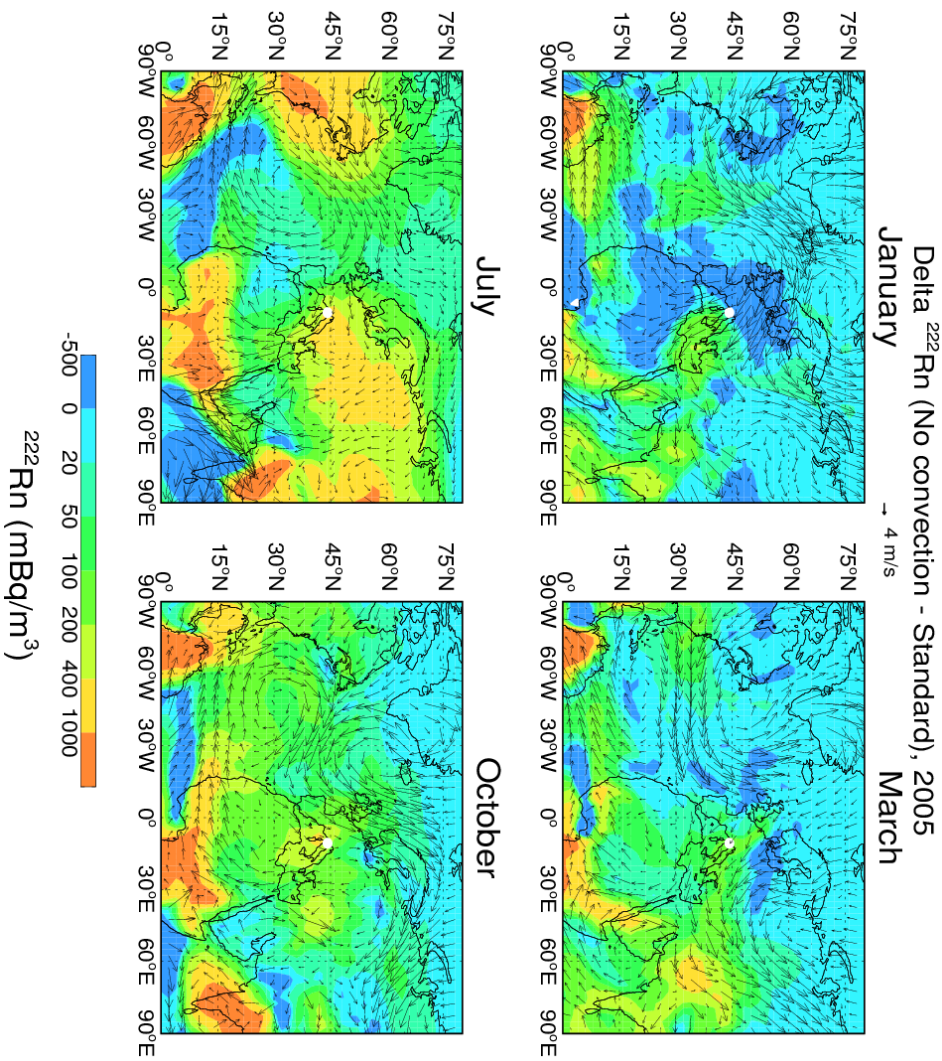
SI Figure 2. Same as SI Figure 1(a, b), but for the “ij-1” grid to the south of Mt. Cimone (left column) and the “i-1j-1” grid to the southwest of Mt. Cimone (right column), respectively.



SI Figure 3. Comparison of GMI simulated monthly percentage fluctuations of ^{210}Pb and ^7Be at Mt. Cimone (“ij-1” grid) between the standard (black dotted line) and the sensitivity runs. The sensitivity runs are those without convective transport/scavenging (red dotted line), without dry deposition (blue dotted line), and without scavenging (orange dotted line). The observations are shown as green solid line.



SI Figure 4. Simulated monthly mean ^{222}Rn concentrations, at the elevation of Mt. Cimone. Arrows represent the seasonality of winds in the MERRA meteorological data. The white dot indicates the location of Mt. Cimone (44°12' N, 10°42' E, 2165 m asl).



SI Figure 5. GMI simulated differences of ^{222}Rn concentrations at the elevation of Mt. Cimone between a sensitivity run without convection and the standard run. Arrows denote MERRA winds. The white dot indicates the location of Mt. Cimone (44°12' N, 10°42' E, 2165 m asl).